Title

Discovery of compounds that reactivate p53 mutants in vitro and in vivo

Journal

Cell Chemical Biology, 29(9)

ISSN

2451-9456

Authors

Durairaj, Geetha

Demir, Özlem

Lim, Bryant

et al.

Publication Date

2022-09-01

DOI

10.1016/j.chembiol.2022.07.003

Peer reviewed

Discovery of Compounds that reactivate p53 mutants in vitro and in vivo

Geetha Durairaj[±],
Department of Biological Chemistry, University of California, Irvine, Irvine, 92697, California, USA

Chao Family Comprehensive Cancer Center, University of California, Irvine, Irvine, 92697, California, USA

Özlem Demir[±],
Department of Chemistry and Biochemistry, University of California, San Diego; La Jolla, California 92093, USA

Bryant Lim,
Department of Chemistry, University of California, Irvine, Irvine, 92697, California, USA

Roberta Baronio,
Department of Biological Chemistry, University of California, Irvine, Irvine, 92697, California, USA

Delia Tifrea,
Department of Pathology and Laboratory Medicine, University of California, Irvine, 92697, California, USA

Linda V. Hall,

[*]Correspondence: pkaiser@uci.edu, ramaro@ucsd.edu.
[±]Equal Contribution
[#]Lead contact

Author contributions:
G.D. and Ö.D. contributed equally to research design. P.K., S.R. and R.E.A. contributed equally to research direction Ö.D., F.S., R.E.A. and R.H.L. designed and directed the computational and studies. G.D. designed and executed the genetics and biochemical experiments. L.L. and M.F.J.F did biochemical experiments. R.B., L.V.H., and D.-W.L. did the genetic studies. J.C.D and B.L. prepared the compounds. Ö.D conceived and ran the virtual screening targeting the L1/S3 pocket. J.K.L purified recombinant p53. C.Y. ran and processed MS data. D.T. handled mice injections and tumor measurements. H.B. analyzed metabolites in tumor samples and C. J. directed the metabolomics experiments. G.D. wrote the manuscript with contributions from Ö.D. and P.K.

Present Address
Roberta Baronio Nuffield Department of Medicine, University of Oxford, Old Road Campus, Roosevelt Drive, Headington, Oxford, OX3 7FZ, UK
Jacob C DeForest Pfizer Inc.,10555 Science Center Dr, San Diego, CA 92121
Faezeh Salehi Adobe, 345, Park Avenue, San Jose, CA 95110
Da-Wei Lin Ambry Genetics, 1 Enterprise, Aliso Viejo, CA 92656

Competing interests:
Several authors of this manuscript are listed as inventors on the patent listed below. The patent describes compounds reported in this manuscript.
Amaro, R. E., Baronio, R., Demir, O., Kaiser, P., Lathrop, R. H., Salehi-Amiri, S.-F., Wassman, C., Patent, “Small molecules to enhance p53 activity”, US20160193214 A1, United States. (Approved: March 2017).

Inclusion and diversity
One or more of the authors of this paper self-identifies as an underrepresented ethnic minority in science. One or more of the authors of this paper self-identifies as a member of the LGBTQ+ community.

Department of Biological Chemistry, University of California, Irvine, Irvine, 92697, California, USA

Jacob C. DeForest,
Department of Chemistry, University of California, Irvine, Irvine, 92697, California, USA

Linda Lauinger,
Department of Biological Chemistry, University of California, Irvine, Irvine, 92697, California, USA

Maryam M. Jebril Fallatah,
Department of Biological Chemistry, University of California, Irvine, Irvine, 92697, California, USA

Clinton Yu,
Department of Physiology and Biophysics, University of California, Irvine, CA 92697, USA.

Department of Developmental and Cell Biology, University of California, Irvine, CA 92697, USA

Hosung Bae,
Department of Biological Chemistry, University of California, Irvine, Irvine, 92697, California, USA

Da-Wei Lin,
Department of Biological Chemistry, University of California, Irvine, Irvine, 92697, California, USA

Jin Kwang Kim,
Department of Biological Chemistry, University of California, Irvine, Irvine, 92697, California, USA

Faezeh Salehi,
Department of Computer Science, University of California, Irvine, Irvine, 92697, California, USA

Cholsoon Jang,
Department of Biological Chemistry, University of California, Irvine, Irvine, 92697, California, USA

Feng Qiao,
Department of Biological Chemistry, University of California, Irvine, Irvine, 92697, California, USA

Richard H. Lathrop,
Department of Computer Science, University of California, Irvine, Irvine, 92697, California, USA

Department of Biomedical Engineering, University of California, Irvine, Irvine, 92697, California, USA

Lan Huang,
Department of Physiology and Biophysics, University of California, Irvine, CA 92697, USA.

Department of Developmental and Cell Biology, University of California, Irvine, CA 92697, USA

Robert Edwards,
Department of Pathology and Laboratory Medicine, University of California, Irvine, 92697, California, USA

Scott Rychnovsky,
Department of Chemistry, University of California, Irvine, Irvine, 92697, California, USA

Rommie E. Amaro*,
Department of Chemistry and Biochemistry, University of California, San Diego; La Jolla, California 92093, USA

Peter Kaiser[*,#]
Department of Biological Chemistry, University of California, Irvine, Irvine, 92697, California, USA

Chao Family Comprehensive Cancer Center, University of California, Irvine, Irvine, 92697, California, USA

Summary

The tumor suppressor p53 is the most frequently mutated protein in human cancer. The majority of these mutations are missense mutations in the DNA binding domain of p53. Restoring p53 tumor suppressor function could have a major impact on the therapy for a wide range of cancers. Here we report a virtual screening approach that identified several small molecules with p53 reactivation activities. The UCI-LC0023 compound series was studied in detail and was shown to bind p53, induce a conformational change in mutant p53, restore the ability of p53 hotspot mutants to associate with chromatin, reestablish sequence specific DNA binding of a p53 mutant in a reconstituted *in vitro* system, induce p53-dependent transcription programs, and prevent progression of tumors carrying mutant p53, but not $p53^{null}$, or $p53^{WT}$ alleles. Our study demonstrates feasibility of a computation guided approach to identify small molecule corrector drugs for p53 hotspot mutations.

eTOC Blurb

A large fraction of human tumors inactivates the major tumor suppressor p53 by mutations. Corrector drugs reactivating mutant p53 are of high clinical value for cancer therapy. Durairaj et al. identify small drug-like compounds that restore wild-type activity to mutant forms of p53 and exhibit anti-tumor effects.

Graphical Abstract

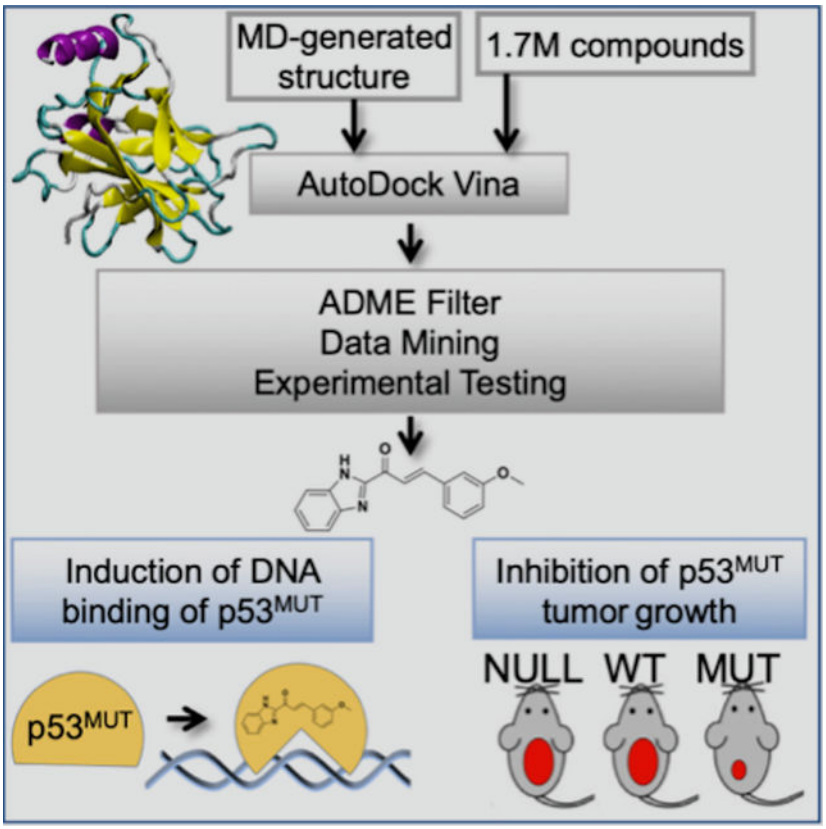

Introduction

TP53 is the most frequently mutated gene in a large fraction of human cancers. Interestingly, a majority (74%) of these TP53 mutations are specific missense mutations that occur at six hotspot residues (R175, G245, R248, R249, R273 and R282) within the p53 DNA-binding region. Missense mutations in p53 generate a defective but abundant p53 protein (Sigal and Rotter, 2000). In addition to abrogating wild-type p53's tumor suppressor function, several missense mutations also confer mutation-specific novel functions that contribute to enhanced tumorigenesis (Brosh and Rotter, 2009; Freed-Pastor and Prives, 2012; Oren and Rotter, 2010). The gain-of-function p53 mutants promote tumor progression by a variety of mechanisms including the loss of its sequence specific DNA binding ability and inactivation of tumor proteins like p63 and p73 (Bargonetti and Prives, 2019).

Tumor maintenance and progression requires inactive p53 (Beraza and Trautwein, 2007; Martins et al., 2006; Ventura et al., 2007). Therefore, pharmaceutical reactivation of p53 cancer mutants stands as an attractive strategy for cancer therapy. Restoring wild-type function to mutant p53 should both eliminate the oncomorphic gain-of-function conferred by mutant p53 and re-enable tumor suppressor function. In recent literature, a handful of promising drug leads have been proposed to restore function to mutant p53 (Beraza and Trautwein, 2007; Bykov et al., 2002, 2005; Wassman et al., 2013; Yu et al., 2012a; Zache et al., 2008). The pioneering and most well-studied of these compounds, APR-246, a derivative of PRIMA-1, has advanced to several clinical studies. In addition, the recently

identified allele-specific p53 reactivation compound NSC319726 was shown to reduce tumor burden in xenograft models expressing the $p53^{R175H}$ hotspot mutant (Yu et al., 2012a). NSC319726 was shown to function via its zinc-ion chelating properties and redox changes, although more recently the copper chelating properties of this compound were shown to be important for reactivation of mutant p53 (Shimada et al., 2018). Lastly, an elegant series of experiments recently showed how arsenic trioxide reacts with 3 cysteine residues in p53 to stabilize the active p53 (Chen et al., 2021). These successes demonstrate feasibility and efficacy of pharmaceutical reactivation of mutant p53.

Although several mutant p53 reactivating small molecules have been identified, rapid progress towards such therapies is hampered by the lack of effective strategies to identify reactivation compounds, the limited mechanistic understanding of pharmaceutical reactivation of mutant proteins, and pharmacological liabilities of current compound classes, such as thiol reactivity and metal chelation (Blanden et al., 2015; Lambert et al., 2009; Yu et al., 2012). Additional classes of compounds with defined mode of actions are therefore highly desired. In this study, we applied an ensemble-based virtual screening approach that has the potential to identify compounds with increased cancer killing potential and with a broad spectrum of activity across a panel of p53 mutants. We show that our compounds bind mutant p53 and change mutant p53 conformation to wild type like structures, restore p53 DNA binding activity *in vitro* and *in vivo* to activate the p53 transcriptional response, which in turn prevents tumor progression in mouse models selectively for tumors with a p53 hotspot mutation.

Results

Identification of small molecules that restore mutant p53 activity by a virtual screen targeting the cryptic L1/S3 pocket of p53

In a quest for p53-reactivating small molecules, we performed a large virtual screen targeting the cryptic L1/S3 pocket. Our prior proof-of-concept study showed that the L1/S3 pocket is located in a region that is enriched with intragenic second-site mutations that can compensate for activity defects associated with several p53 cancer mutations (Wassman et al., 2013). We therefore reasoned that this region is susceptible to conformational changes that can restore activity to p53 mutants when bound to optimal small molecules (Wassman et al., 2013). As the L1/S3 pocket is closed in all p53 crystal structures (Fig. 1A), we used the molecular-dynamics-generated open conformation of the pocket (Fig. 1B) to virtually screen the ZINC Leads Now library (a curated library of commercially-available compounds) of approximately 1.7 million compounds for binding using Autodock Vina (Trott and Olson, 2009) (Fig. 1C). Compounds with the top-ranked 1% docking scores (17,387 compounds) were filtered for ADME properties in Schrodinger suite (QikProp, version 3.3, Schrödinger, LLC, New York, NY, 2010) resulting in 9,668 compounds for further datamining (Fig. S1A and S1B). An additional docking score was obtained for each of these 9,668 compounds using Surflex (Jain, 2007). Of the 9,668 compounds, 138 were selected for experimental testing, using the following criteria i) docking scores, ii) cost, and iii) structural diversity. The full predicted library contains several hundred more compounds with similar rankings, which are available for datamining in the future.

To validate our computationally identified compounds experimentally, we treated human osteosarcoma Saos-2 cells harboring different p53 mutations with the predicted compounds. Saos-2 cells lack p53 but were engineered to have doxycycline-inducible expression of either wild-type p53 or the most frequent p53 mutant found in human cancers, R175H (Leroy et al., 2013; Wassman et al., 2013). Induction of wild type p53, but not mutant p53, prevents cell proliferation of Saos-2 cells (Wassman et al., 2013). p53 reactivation compounds can be distinguished from general cytotoxic compounds through differential effects on parental $p53^{null}$ Saos-2 and the derived $p53^{R175H}$ cells. The use of these engineered cell lines with identical genetic background increases confidence in compound action on p53 mutants because different compound susceptibility due to genetic modifiers can be excluded. Fourteen of 138 computationally predicted p53 reactivation compounds demonstrated a selective effect on cells expressing $p53^{R175H}$ (Fig. 1D and 1E, Supplementary Table S1) compared to $p53^{null}$ cells. We expanded this assay to additional common p53 cancer hotspot mutations (G245S, R248W, and R273H). Numerous compounds showed activity towards several p53 mutants, suggesting a broad activity spectrum (Fig. 1F). In addition, several compounds also induced p53 specific gene expression in p53 hotspot mutants upon treatment (Fig. S1C). APR-246, a derivative of PRIMA-1 was tested in parallel to compare its activity with compounds reported in this study (Fig.S1C).

UCI-LC0023 series of compounds corrects defects of multiple p53 mutants

To understand the mechanism underlying the anti-proliferative activity, we selected UCI-LC0023 (27UDP in Fig 1) for further analysis and development. Most p53 cancer hotspot mutants responded to UCI-LC0023, both in the isogenic Saos-2 background, ovarian and breast cancer cell lines, whereas $p53^{null}$ cells and cells carrying wild-type p53 (MCF7) were less responsive (Fig. 2A, Fig. S2A).

To confirm that the antiproliferative effects of UCI-LC0023 is mediated through reactivation of p53 and not via p53 family member, p73, we generated p73 knockdowns in TOV112D cells. Knockdown of p73 did not alter sensitivity to UCI-LC0023 demonstrating that the effect of UCI-LC0023 is independent of p73 (Fig. S2B).

We generated several derivatives of UCI-LC0023 with a focus on improving solubility and probing structural tolerance. These modifications altered two aspects of UCI-LC0023, the benzimidazole and the substituent at the 3-position of the phenyl ring (Fig. 2B). The benzimidazole of UCI-LC0023 was substituted for other similar heterocycles (indoles, benzofurans, and benzothiophenes). However, none of these heterocycles were effective in increasing the activity of the compounds relative to that of the corresponding benzimidazoles (Fig. 2C). Thus, the benzimidazole moiety was maintained. The relatively poor solubility of UCI-LC0023 prompted us to explore other substituents (–H, –F, –Br, –CH3, –CF3, and –OCH3). Among these substituents, the – OCH3 substituted analog (UCI-LC0019) exhibited significantly increased solubility while maintaining activity and selectivity (Fig. 2C). These experiments provided some insight into structure activity relations as well as information on structures important for p53 specific effects.

The most advanced p53 reactivating compounds are PRIMA-1 and its derivative APR-246, which is currently in clinical trial (Bykov et al., 2002; Cluzeau et al., 2021; Lambert et al., 2009; Lehmann et al., 2012; Sallman et al., 2021). We therefore compared APR-246 with UCI-LC0023 and one of its derivatives, UCI-LC0019, which we used in xenograft experiments as described below. TOV112D ovarian cancer cells ($p53^{R175H}$) were treated with different concentrations of compounds and cell numbers were determined after 1, 2, and 3 days (Fig. 3A). The effect of APR-246 was significantly delayed as compared to UCI-LC0019 and UCI-LC0023. To evaluate the respective contributions of cell cycle arrest and apoptosis to the observed reduced cell number, we performed Annexin V and propidium iodide staining followed by flowcytometric analyses (Fig. 3B). To directly compare compound activity, cells were treated with a dose reflecting two-fold the dose that generated an IC_{50} after 72 hours of growth with the compound. Similar to the growth assay (Fig. 3A), UCI-LC0019 and UCI-LC0023 rapidly induced apoptosis, whereas APR-246 acted more slowly (Fig. 3B).

The comparison of UCI-LC0023 with APR-246 revealed a different kinetic of compound effects, which likely indicates diverse mode of actions.

UCI-LC0023 directly binds to mutant p53

We next attempted to map the binding site of UCI-LC0023 on p53. To this end we synthesized the photo-affinity labeling enabled diazirine analog UCI-LC0045, which maintained the activity of the parent compound in cell-based assays (Fig. 3C). UCI-LC0045 was incubated with the recombinant purified $p53^{R175H}$ DNA binding domain, the compound activated by UV, tryptic peptides generated, and analyzed by mass spectrometry. A peptide containing cysteine 124 (C124), which sits at the center of the L1/S3 pocket, was the only photo-linked peptide that was identified at low compound concentrations (Fig. S3A and Fig. 3D). The fragmentation map was consistent with amino acids 123–126 as potential crosslinked residues, but UCI-LC0045 was most likely photo-linked to C124, because all other cysteine residues could be alkylated during sample preparation for mass spectrometric analyses, indicating that C124 was protected by covalently linked UCI-LC0045. Higher concentrations of UCI-LC0045 resulted in two additional photo-labeled peptides, but the C124-containing peptide remained by far the most enriched binding site at all compound concentrations (Fig. S3B and Supplementary Table S2). These results corroborate the computational prediction and indicate direct binding of UCI-LC0045 to the L1/S3 region of p53. No covalent linkage of UCI-LC0045 to p53 was detected without UV activation (Supplementary Table S3). This is important because this compound series contains a potential Michael acceptor, which could alkylate cysteine residues. Indeed, the best-studied p53 reactivation compound, PRIMA-1 (Bykov et al., 2002), acts through a covalent mechanism and links to cysteines 124 and 277 in p53 (Wassman et al., 2013; Zhang et al., 2018). Cysteine 124 was also implicated in binding arsenic trioxide (Chen et al., 2021). Interestingly, our computational approach initially predicted C124 as the functionally important attachment site for PRIMA-1 (Wassman et al., 2013). Consistent with these predictions, substitution of C124 with alanine blocked PRIMA-1 mediated p53 reactivation (Wassman et al., 2013; Zhang et al., 2018). In contrast, and consistent with a non-covalent

mode of action, the C124A substitution did not affect reactivation of $p53^{R175H}$ by UCI-LC0023 (Fig. 3E).

Thiol reactivity is not involved in the mode of action for the UCI-LC0023 compound series

Experiments using p53 C124A mutants confirm that the UCI-LC0023 compound series does not reactivate through a covalent mechanism that involves cysteine 124 in p53 (Fig. 3E). The lack of any detectable cysteine reactivity without UV activation of UCI-LC0045 further supports that this compound series does not efficiently react with cysteine residues in proteins (Supplementary Table S3). Nevertheless, we wanted to test whether thiol reactivity *in vivo* might contribute to the observed inhibition of cell proliferation of UCI-LC0023 and of UCI-LC0019. This question is critical because despite extensive research on PRIMA-1 and APR-246, recent studies suggested that the mode of action of APR-246 is not via reactivation of p53, but rather through its effect on the redox pathway due to covalent modification of cysteines (Liu et al., 2017; Peng et al., 2013). Most importantly, the antiproliferative effect of APR-246 on p53 mutant cells was linked to depletion of the important cellular anti-oxidant glutathione. Methylene quinuclidinone, a degradation product of APR-246 was shown to covalently attach to the critical cysteine residue in glutathione and therefore reduce the ability to defend cells against oxidative insult (Liu et al., 2017). Accordingly, the effects of APR-246 on cell proliferation can be quenched by exogenous supply of the cell permeable anti-oxidant N-acetyl-cysteine (NAC). To test whether the mode of action of UCI-LC0023 and UCI-LC0019 is similar to that of APR-246 we treated TOV112D cells with compounds in the presence of NAC. Consistent with previous reports (Liu et al., 2017), NAC potently suppressed anti-proliferative effects of APR-246 (Fig. 4A). In contrast, treatment with NAC did not rescue the growth inhibition of TOV112D cells mediated by UCI-LC0019 (Fig. 4B) or UCI-LC0023 (Fig. 4C) confirming that this compound series acts through a mechanism distinct from APR-246 and other thiol reactive p53 reactivation compounds.

UCI-LC0023 restores “WT-like” conformation of mutant $p53^{R175H}$

Because UCI-LC0023 binds to p53 and prevents cancer cell proliferation, we next wanted to investigate if UCI-LC0023 restored a “WT-like” conformation to $p53^{R175H}$ mutants. Compound-induced conformational changes can be monitored by a set of conformation-specific antibodies that selectively recognize the wild-type conformation (PAB1620) or the altered conformation of the $p53^{R175H}$ mutant (PAB240) (Yu et al., 2012b). Treatment of TOV112D cells with UCI-LC0023 increased the detection with wild-type specific antibodies and decreased the $p53^{R175H}$ mutant specific signal (Fig. 4D). The signal decrease in detection of the mutant conformation appears to be more drastic than the increase of wild-type conformation. This is consistent with previous experiments and may be due to the generally weaker signal of PAB1620 (Liu et al., 2013; Yu et al., 2012). It could also be a reflection of the general nature of compound-based p53 mutant reactivation, which may induce a partial reversion to the wild-type conformation. Consistent with the imaging results, incubation of TOV112D cell lysates with UCI-LC0023 diminished immunopurification with the mutant p53 selective PAB240 antibody (Fig. 4E). Together, these results indicate that UCI-LC0023 triggers a conformational change in $p53^{R175H}$ towards a wild-type like structure *in vivo*.

UCI-LC0023 restores DNA binding of p53 mutants *in vitro* and *in vivo* and induces p53 target gene expression

p53 is a transcription factor whose DNA binding is crucial for performing its functions (Laptenko and Prives, 2006; Sullivan et al., 2018). $p53^{R175H}$ is a structural mutation that has been shown to impair its ability to bind DNA (Aggarwal et al., 2016). We therefore examined if UCI-LC0023 can restore DNA binding properties to the $p53^{R175H}$ mutant. Treatment of TOV112D cells ($p53^{R175H}$) with UCI-LC0023 resulted in rapid redistribution of $p53^{R175H}$ to the chromatin fraction (Fig. 5A and Fig. 5B). In contrast, APR-246 did not induce redistribution of $p53^{R175H}$ to the chromatin fraction (Fig. S4A). UCI-LC0023 induced redistribution to chromatin was also observed in other engineered Saos-2 cells with inducible expression of several p53 mutants (R175H, Y220C, R248W, R282W, R273H, G245S) (Fig. 5C), and breast cancer p53 mutant cell line MB231 (R280Q) (Fig. S4B). The inactive derivative UCI-LC0014 did not restore chromatin binding of p53 mutant in TOV112D cells (Fig. S4C). Although, we largely excluded cysteine reactivity as a mode of action for UCI-LC0023, we considered a potentially indirect effect through Crm1 inhibition in this assay. The nuclear export factor Crm1 is effectively inhibited by cysteine reactive compounds (Ferreira et al., 2020), which could contribute to the observed effects. However, the Crm1 inhibitors KPT-185 and leptomycin B had no effect on chromatin binding of $p53^{R175H}$ (Fig. S4D, E, and F), and UCI-LC0023 did not affect localization of the Crm1 substrate and p53 homolog p73 (Fig. S4G). While these results indicate the ability of UCI-LC0023 to restore DNA binding activity to p53 hotspot mutants, this method cannot distinguish between a direct and indirect mode of action. We therefore evaluated the restoration of site-specific DNA binding of mutant p53 in a purified reconstituted system.

The recombinant purified DNA binding domains of $p53^{WT}$ and $p53^{R175H}$ were incubated with biotinylated DNA fragments representing the p53 binding site of the *GADD45A* gene (El-Deiry et al., 1992) or a p53-independent promoter region. The DNA/p53 complex was purified on streptavidin beads and analyzed by immunoblotting. UCI-LC0023 restored sequence selective binding of $p53^{R175H}$, albeit some non-selective DNA binding was also observed (Fig. 5D). These results demonstrate that the UCI-LC0023 is sufficient to correct the DNA binding defect of $p53^{R175H}$. Together, DNA and chromatin binding results indicate that we have identified a small molecule that directly restores DNA binding activity of mutant p53 *in vitro* and *in vivo*. Consistent with these results, UCI-LC0023 induced restoration of site-specific DNA binding of the $p53^{R175H}$ mutant to the promoters of the p53 dependent genes p21 and PUMA in TOV112D cells as demonstrated by chromatin immunoprecipitation (ChIP) (Fig. 5E). Treatment with UCI-LC0023 also resulted in induction of a p53 specific gene expression program (Fig. 5F and 5G). Interestingly, when we examined the effects of UCI-LC0023 on expression changes in TOV112D cells ($p53^{R175H}$) on a custom designed p53 Nano String panel, we not only observed induction of p53 target genes, but also downregulation of genes associated with the oncomorphic gain-of-function properties of mutant p53 (Fig. 5G). Together these experiments support that UCI-LC0023 restores the DNA binding of p53 mutants *in vitro* and *in vivo* and induces expression of target genes.

Anti-tumor activity of UCI-LC0019 in Xenograft Tumor models

To investigate the antitumor effect of the UCI-LC0023 compound series *in vivo*, xenograft mouse tumors were generated by inoculating mice with cells derived from human tumor cell lines carrying wild type p53 (HCT116), $p53^{R175H}$ (TOV112D), and $p53^{null}$ ($TOV112D^{p53-/-}$). $TOV112D^{p53-/-}$ was generated by CRISPR knockout of the $p53^{R175H}$ allele in TOV112D cells (Fig. S5F and Fig. S5G). Due to poor solubility of UCI-LC0023, we chose the methoxy derivative UCI-LC0019 for mouse experiments. UCI-LC0019 was synthesized using a focused library approach around the scaffold of UCI-LC0023 and maintained similar activity and properties, but with improved solubility (Fig. 2C, Fig. 3A, Fig. 3B, Fig. 4B, Fig. S5A, Fig. S5B and Fig. S5C). Upon formation of palpable tumors, intraperitoneal injections of UCI-LC0019 were administered daily at a dose of 10mg/kg or 3.3mg/kg (Fig.S5D). Treatment with UCI-LC0019 resulted in a significant reduction of tumor volume in $p53^{R175H}$ carrying TOV112D tumors (Fig. 6A, S5D, S5E). Importantly, UCI-LC0019 did not significantly inhibit the growth of $TOV112D^{p53-/-}$ or HCT116 ($p53^{+/+}$) tumors (Fig. 6B, 6C, S5G, S5H), strongly suggesting that the anti-tumor effects of UCI-LC0019 were due to reactivation of $p53^{R175H}$ *in vivo*. Treatment with UCI-LC0019 did not result in weight loss or any obvious toxic effects (Fig. S4F). Some putative p53 reactivation compounds, particularly the clinical PRIMA-1 derivative APR-246, were suggested to primarily act through covalent conjugation to glutathione. Reduced glutathione levels and hypersensitivity to oxidative environments may thus significantly contribute to the mode of action of APR-246 and other cysteine reactive compounds (Liu et al., 2017). We therefore analyzed tumor samples from mice treated with UCI-LC0019 by mass spectrometry (Fig. 6D). Glutathione levels were not depleted, but did increase in response to UCI-LC0019, excluding glutathione depletion as a mode of action as well as indicating an intact glutathione regulatory pathway. These findings provide strong *in vivo* evidence for a mode of action that depends on p53 mutants. Together with the presented *in vitro* evidence, the mouse experiments support that the UCI-LC0023 compound series binds mutant p53, thereby inducing a wild-type like conformation and activity, which restores critical aspects of p53 tumor suppressor function to prevent tumor progression.

Discussion

Many tumors express high levels of full-length, but mutated p53 that no longer suppresses tumor progression. Reactivation or correction of p53 mutants is thus viewed as a promising pharmacological approach for cancer treatment. Unlike conventional targeted cancer drugs that work by inhibiting protein function, p53 restoration requires a functional reconstitution rather than inhibition. In addition to restoring the p53 tumor suppressor activity, p53 reactivating small molecules are also expected to inhibit the gain-of-function oncomorphic properties of mutated p53. Thus, pharmaceutical reactivation of p53 mutants is very challenging. Experience in the development of corrector drugs is scarce (Habib et al., 2019), but pioneering work on PRIMA-1 and thiosemicarbazones have demonstrated feasibility and stimulated efforts towards p53 reactivation drugs (Bykov et al., 2002; Yu et al., 2012b). Most recently, arsenic trioxide was also shown to correct folding defects of p53 mutants by engaging three cysteine residues (Chen et al., 2021). Notably, C124 is required for corrector function of arsenic trioxide and is located in the cryptic L1/S3 pocket we have

targeted in this study. Pharmacological liabilities such as thiol reactivity of PRIMA-1 and arsenic trioxide, requirement of metal binding for thiosemicarbazones, general toxicity of arsenic compounds, and uncertainty about *in vivo* mode of action of available compounds, necessitate continued efforts to identify and develop additional chemically diverse small molecule leads for the development of p53 reactivation drugs. In this study, we report a computational approach to target the L1/S3 pocket in p53 that was guided by our genetic studies on mutational reactivation (Wassman et al., 2013). We identified several compounds that showed activity towards several p53 hotspot mutants suggesting a broad activity spectrum, which is consistent with mutational studies that showed structural changes introduced by rescue mutations in the L1/S3 region to restore activity of multiple p53 mutations (Wassman et al., 2013). It was however surprising that both conformational (class II) (R175, G245, R249) and DNA contact (class I) (R248, R273, R282) hotspot mutants (Freed-Pastor and Prives, 2012) are responsive to several of the compounds targeting the L1/S3 pocket. Arsenic trioxide appears to primarily correct defects of conformational mutants (Chen et al., 2021), albeit not all mutants have been classified in this manner. It will be very interesting to explore this question mechanistically, because the only well-understood mechanism for restoring class I mutants are mutations that introduce a new DNA contact site, such as the S240R mutation (Eldar et al., 2013). However, other mechanisms do exist because rescue mutations for p53 class I mutants that are distant from the DNA interacting surface have also been reported and must follow different mechanisms, perhaps by transmitting structural changes that change the DNA contact conformation (Baronio et al., 2010). In addition, non-canonical mechanisms for p53-dependent tumor suppression have been suggested, which may require different DNA contacts (Li et al., 2012). Notably, PRIMA-1 and APR-246 have also been suggested to restore activity of both p53 conformational and DNA contact mutants, and the L1/S3 pocket is one of the proposed binding sites for PRIMA-1/APR-246 (Wassman et al., 2013; Zhang et al., 2018). Overall, a remarkable property of targeting the L1/S3 pocket is that it appears to present a universal reactivation or corrector site in p53 as both rescue mutations located in this region as well as the small molecules we present here, seem to rescue multiple p53 cancer mutations.

We observed that the mechanism through which the UCI-LC0023 series of compounds reactivate mutant p53 appears to involve direct binding of the compounds to mutant p53 protein. We propose a model for this compound series where compound binding to the L1/S3 pocket induces a conformational change that resembles the active p53 protein. The p53 mutant/compound complex regains tumor suppressor function and suppresses oncomorphic gain-of-function properties associated with p53 hotspot mutations. This model is supported by biochemical experiments as well as cell and animal studies. Most importantly, reconstitution of compound-restored *in vitro* DNA binding demonstrates the direct mode of action for the UCI-LC0023 compound series (Fig. 5D). Many of the putative p53 reactivation compounds reported in the literature have not been shown to bind p53 and the anti-cancer effects of some of the compounds have been attributed to compound effects that were independent of p53 reactivation (Gottlieb et al., 2017; Lu et al., 2016; Mobaraki et al., 2018; Patyka et al., 2016; Peng et al., 2013; Yoshikawa et al., 2016). In particular the large class of thiol reactive compounds such as PRIMA-1 and its clinical derivative APR-246 have recently been suggested to act mainly through induction of redox imbalance

by depletion of glutathione (Liu et al., 2017). Accordingly, cell permeable anti-oxidants such as N-acetylcysteine can overcome the effects of thiol reactive p53 reactivators (Liu et al., 2017) (Fig. 4A). Importantly, we can exclude such a mechanism for the UCI-LC0023 compound series, because N-acetylcysteine had no effect on activity of these compounds (Fig. 4B and C). Evidence for a direct reactivation mechanism of the UCI-LC0023 series comes from mass spectrometric analysis of a diazirine analog that demonstrated binding of UCI-LC0023 to p53. It must be noted that evidence has also been reported for physical interactions between cysteines 124 and 277 of p53 and PRIMA-1/APR-246, and this interaction contributes to the antiproliferative effects of PRIMA-1/APR-246 in tissue culture (Wassman et al., 2013; Zhang et al., 2018). More recently multiple crystal structures of p53 with the active APR-246 degradation product 2-methylene-3-quinuclidinone (MQ) attached to six different cysteine residues were reported and may explain some of the structural changes that could contribute to APR-246 mediated p53 reactivation (Degtjarik et al. 2021). However, such MQ-p53 conjugates have not been confirmed in vivo, and the biological relevance of these in vitro conjugates remains to be addressed. Nevertheless, it is possible that N-acetylcysteine may quench the PRIMA-1/p53 interaction and thereby suppress compound effects, but non-specific effects of PRIMA-1 and APR-246 that affect redox balance likely have a significant contribution to the effects of these compounds (Liu et al., 2017; Peng et al., 2013). The UCI-LC0023 series of compounds have an enone that can also potentially form covalent attachments to surface exposed cysteine residues in proteins. However, we did not detect any covalent compound-p53 interactions even when very high concentrations of compound were incubated with p53. In addition, and in contrast to PRIMA-1/APR-246, UCI-LC0023 restored activity of $p53^{R175H}$ even when cysteine 124 was mutated to alanine (Wassman et al., 2013; Zhang et al., 2018) (Fig. 3E), and was not affected by N-acetylcysteine (Fig. 4C). Furthermore, no depletion of glutathione was observed in tumors isolated from mice treated with UCI-LC0019 (Fig. 6D). This difference is likely due to the higher reactivity of the Michael acceptor found in PRIMA-1/APR-246, which exhibits an exocyclic alkene that is more sterically accessible to nucleophiles such as cysteine. Additionally, while addition into the Michael acceptor of the UCI-LC0023 series of compounds may also be facile, elimination of the thiolate is thermodynamically driven by restoration of conjugation between the ketone and arene ring. This elimination is likely the reason why unlike PRIMA-1/APR-246, these compounds do not exhibit observable covalent attachment to p53.

UCI-LC0023 restored DNA binding and transactivation functions to mutant p53. Using chromatin fractionation studies, we demonstrated that UCI-LC0023 restores DNA binding across several p53 mutants. To ensure that such restoration of DNA binding was direct and not mediated via other factors, we examined UCI-LC0023 induced DNA binding in a reconstituted system *in vitro*. UCI-LC0023 was able to induce specific DNA binding of purified recombinant $p53^{R175H}$ *in vitro*, thereby providing strong evidence for the direct mode of action we propose for UCI-LC0023. To the best of our knowledge, such *in vitro* reactivation in a system that contains only DNA, p53, and compound has not been achieved with any other p53 reactivation compound and provides very strong support for a direct mode of action. Stimulation of $p53^{R175H}$ mutant protein binding to a canonical p53 binding site of GADD45A was very strong, but we also observed a small increase of non-specific

DNA binding (Fig. 5D). This is perhaps not unexpected because complete reversion to wild-type behavior cannot be presumed. Whether off-target activation mediated by compound action occurs *in vivo*, and if the potential off-target binding recognizes preferred sequences will be interesting questions to explore in the future. The lack of obvious adverse effects in mice suggests that these potential non-specific DNA interactions do not impact overall health of the organism.

Strong evidence suggests that certain p53 cancer mutants directly or indirectly activate oncogenic genes, which contribute to tumor progression and explains the dominance of p53 missense mutations over nonsense mutations or p53 deletions in human cancer (Bargonetti and Prives, 2019). Our results indicate that in addition to reactivating mutant p53 to regain its wild type activity, UCI-LC0023 may also reverse the oncogenic properties of mutant p53. Therefore, these results have direct implications on the therapeutic value of p53 reactivation compounds as they not only restore tumor suppressor function (e.g. transcription of NOXA, p21), but also overcome “gain-of- function” activity of mutant p53 (e.g. repression of MLL1, MOZ, Dicer, c-MYC). While other compounds such as HDAC inhibitors can also induce p21 and NOXA expression, several additional p53-dependent genes are responsive to UCI-LC0023 treatment (Fig. 5G) and compound treatment induced p53 binding to target promoters in vivo (Fig. 5E), suggesting that expression effects are triggered by reactivation of mutant p53.

Although it is evident that the UCI-LC0023 compound series shows selective killing of cancer cells that express p53 hotspot mutants, these compounds also contain general cytotoxic activity. Through structure activity relationship analyses (Fig. 2C) we could identify regions of the compound that are important for specific effects on p53 mutants, but these limited experiments could not separate general cytotoxicity from mutant p53 selective effects. More extensive chemical development will be important to address this issue. Interestingly, in mice, mutant-p53 specific effects of UCI-LC0019 seem to be much better separated from general cytotoxic effects than in tissue culture settings. This is evident by strong effects of UCI-LC0019 on tumors expressing $p53^{R175H}$ and very subtle effects on the same tumors lacking p53 (Fig. 6 and S5D).

In summary, we report a computational approach that resulted in identification and development of small molecules that bind the L1/S3 pocket of p53 and restore tumor suppressor functions *in vitro* and *in vivo.* Identified compounds act through a well-defined mode of action, do not require covalent attachment, induction of redox imbalance, or metal binding, and have selective anti-cancer activities dependent on p53 missense mutations in tumors. Our study provides a framework for p53 reactivation compound discovery that can help to increase chemical diversity and improve pharmacological properties necessary for translation of pharmaceutical p53 mutant reactivation to the clinic. Future experiments will need to further define the mechanism by which these compounds restore wild-type like properties to p53 hot spot mutations as well as the potential role of Crm1-independent localization changes associated with this process.

Limitation of study

There is a long history of pharmaceutical reactivation of p53 mutants found in cancer, initiated by the seminal study that led to the discovery of PRIMA-1 (Bykov et al., 2002). A number of compounds have since been identified that trigger various p53 controlled processes in cancer cells expressing p53 hot-spot mutants (Hoe et al., 2014; Muller and Vousden, 2014). The mode of action in vivo of many of these compounds seems to be indirect and at least partially due to depletion of glutathione. Although we can exclude glutathione depletion as a mode of action, we cannot fully exclude other indirect effects that could potentially lead to the observations in this report. Further experimental support will be needed in the future.

Significance

Mutations that disrupt the function of the tumor suppressor p53 play an important role in human cancers. Diverse therapeutic approaches are actively pursued to target this pathway. Interestingly, a large fraction of p53 alterations are missense mutations resulting in abundant mutant p53 protein levels in tumors that are in principle amenable to a corrector drug approach. We report a computation-guided approach to identify small molecules that can restore aspects of wild-type p53 function to mutated p53 both in vitro and in vivo. This strategy can increase chemical diversity of p53 corrector molecules for clinical development. The reported approach identified small molecules that restore mutant p53 DNA binding in a purified system demonstrating direct corrector activity in vitro. Although we cannot exclude the contribution of indirect effects to the observed mutant p53 reactivation activities we observe in vivo, indirect redox related mode of actions as seen for several other small molecule p53 reactivators are unlikely to play a role. Despite these advances it remains challenging to define exact mechanisms and develop highly active corrector drugs for mutated p53, but this progress is encouraging given the large number of cancer patients with p53 mutations that could benefit from such drugs.

STAR Methods

RESOURCE AVAILABILITY

Lead contact—Further information and requests for resources and reagents should be directed to and will be fulfilled by the lead contact, Peter Kaiser (pkaiser@uci.edu).

Materials availability—This study did not generate unique reagents.

Data and code availability—The paper does not report original code. Any additional information required to reanalyze the data reported in this paper is available from Rommie Amaro (ramaro@ucsd.edu) upon request. All virtual screening data reported in this paper will be shared by Rommie Amaro (ramaro@ucsd.edu) upon request.

EXPERIMENTAL MODEL AND SUBJECT DETAILS

Mice—NOD.*Cg-Prkdc*^{scid}*Il2rg*^{tm1Wjl}/SzJ, NSG™(branded name). Mice were originally purchased (The Jackson Laboratory,#005557) and bred inhouse. We utilized 5 to 7 weeks old females, maintained in autoclaved cages, in sterile conditions with autoclaved food and

water, according to the approved IACUC protocol AUP 20–033 with expiration date May, 05, 2023. The mice were not used in previous studies and were drug naive. Groups of a minimum 5 were utilized per experimental procedure, and the experiments were repeated at least twice.

Cell lines—Cell lines were either purchased from ATCC and cultured as indicated in the detailed methods section. Saos-2 (osteosarcoma, female), TOV-112D (adenocarcinoma, ovary, female), MCF7 (adenocarcinoma, breast, female), HCT116 (colorectal carcinoma, male), MDA-MB468 (adenocarcinoma, breast, female), MDA-MB231 (adenocarcinoma, breast, female), HCC70 (ductal carcinoma, breast, female),

QUANTIFICATION AND STATISTICAL ANALYSIS

The statistical details can be found in corresponding figure legends. All data are represented as standard deviation of mean or S.E.M. as indicated in the corresponding figure legends. The given 'n' values represent either the number of biological replicates or the number of independent experiments. Statistical analyses were performed using Graphpad prism and Microsoft Excel. For comparison between two groups, data were subjected to the Student's t-test, and for multiple comparisons Turkey's multiple comparisons test, RM ANOVA with Sidak's multiple comparison's test were used. $p < 0.05$ was considered significant.

METHODS DETAILS

Virtual Screen Targeting the L1/S3 pocket.—1,738,752 compounds in the ZINC Leads Now database January 2011 version (http://zinc.docking.org) were virtually screened using Autodock Vina[41] with exhaustiveness value of 8 and energy range value of 4. For docking, the search space is centered at the sulphur atom of Cys124, and has dimensions of 20 Å × 20 Å × 20 Å. For the virtual screening, we used only the cluster 13 "open" representative conformation of the p53 R273H mutant as this receptor conformation proved to be very successful in selecting hit compounds in our proof-of-concept study (Wassman et al., 2013). Based on the Autodock Vina docking scores, the top 1% of the compound library which corresponds to 17,387 compounds is collected and is called "Set V". The distribution of the Autodock Vina docking scores for the top 1% can be found in Fig. S1. Filtering Set V compounds for calculated ADME properties (strict compliance to Rule of 5, Rule of 3, and $\log P_{oct/wat} \leq 3$) in Schrodinger suite left us with a set of 9,668 compounds called "Set A". Additional docking scores were computed for Set A compounds with Surflex program. The docking scores from Autodock Vina and Surflex programs were normalized and a combined (mean) normalized score was calculated for each compound. Leadscope Personal software (www.leadscope.com) was used to classify the 9,668 compounds by their chemical scaffolds. A final set of 138 compounds was selected for experimental testing as a combination of the three sets of compounds below:

A. 46 non-enone compounds, selected from Set A, with the highest combined docking scores and diverse scaffolds, and that were available for purchase;

B. 46 enone compounds, selected from Set A, with the highest combined docking scores and diverse scaffolds, and that were available for purchase;

C. 46 compounds, selected from Set V, with the highest Autodock Vina docking scores, and that were available for purchase and were not selected for the above two sets. Among these 46 compounds, 32 compounds appeared in Set A while 14 compounds did not appear in Set A.

Cell lines—Stable Soas-2 cell lines harboring doxycycline-inducible p53 wild type or mutants were established by a lentivirus-based strategy as previously described (Wassman et al., 2013). Saos-2, HCT116 cells were cultured in Dulbecco's modified Eagle's medium (DMEM) with 10% FBS supplemented with 10% FBS, penicillin G sodium (100 units ml^{-1}) and streptomycin (100 μg ml^{-1}). TOV112D cells were cultured in 1:1 mixture of MCDB 105 medium containing a final concentration of 1.5 g/L sodium bicarbonate and Medium 199 containing a final concentration of 2.2 g/L sodium bicarbonate supplemented with 10% FBS, penicillin G sodium (100 units ml^{-1}) and streptomycin (100 μg ml^{-1}). To generate knockout of $p53^{R175H}$ in TOV112D cells, lentiCRISPRv2 (addgene plasmid #52961) was used(Sanjana et al., 2014). gRNA sequence for the knockout was designed at crispr.mit.edu(Ran et al., 2013). Annealed gRNA was inserted into BsmBI digested lentiCRISPRv2 plasmid. The lentiviral plasmid containing the gRNA sequence was used to generate lentivirus, which was then used to transfect TOV112D cells to generate a knockout of the $p53^{R175H}$ allele to generate $TOV112D^{p53null}$. For p73 knockdown, clones of pLKO.1-shRNAs TRCN0000006507 (shRNA#1) and TRCN0000006508 (shRNA#2) were a gift from Dr. Anand Ganesan, University of California, Irvine. Virus packaged shRNAs were infected into TOV112D cells to generate p73 knockdown cells.

Cell viability—Cells were placed in 96-well plates at a density of 10,000 cells per well and incubated overnight. Doxycycline (final concentration 1 μg/ml) was added to induce the expression of p53 in Saos-2 cells harboring different p53 mutants for 16 hours before the reactivation compounds or vehicle was added to the cultures. Concentration of the compounds used are: 22LSV and 25KKL (100μM); 26RQZ (10μM); 27TGR (75μM); 27UDP and 27VFS (20μM); 27WT9 (10μM); 28NZ6 (50μM); 32CTM (40μM); 32LDE (10μM); 33AG6 (100μM); 33BAZ (50μM); 35LWZ (50μM); 35ZWF (100μM); PRIMA-1 (50μM) and Stictic acid (37μM). PRIMA-1 was preheated to 100°C for 10 min to promote formation of active decomposition products and then cooled before it was used in these experiments. For N-acetyl-cysteine assays, 2000 TOV112D cells per well were used. Concentration of the compounds used were 25μM UCI-LC0019, UCI-LC0023 or 40μM APR-246 in the presence and the absence of 5mM N-acetyl-cysteine (NAC). Cell viability assays were performed using CellTiter-Glo Luminescent Cell Viability Assay (Promega, Wisconsin, MD) according to the manufacturer's instructions. Data represents the average of three independent samples.

Lysate preparation and Western Blot analysis—For tumor xenografts from TOV112D ($p53^{R175H}$) and $TOV^{p53null}$, cells were harvested and lysed in 8M Urea buffer (8 M urea, 200 mM NaCl, 100 mM Tris, pH 7.5, 0.2% SDS, 10 mM Na-pyrophosphate, 5 mM EDTA, 5 mM EGTA, 50 mM NaF, 0.1 mM orthovanadate, 1 mM PMSF, 1 μg/ml each of Aprotinin, leupeptin and pepstatin). 10–15μg of lysates were separated by SDS-PAGE and transferred on to PVDF membranes. The blots were developed using Supersignal west

pico plus chemiluminescent substrate (Thermo Fisher). The antibodies used were p53 (Santa Cruz Biotechnology, FL-393) and GAPDH (Santa Cruz Biotechnology, sc-32233).

Cell fractionation assay—TOV112D and Saos-2 cells harboring various p53 mutants were treated with vehicle (DMSO) or 30μM UCI-LC0023 for 3 hours. For fractionation assay with Crm1 inhibitor KPT-185 (Selleckchem, S7125), cells were treated with 25 nM KPT-185 for 24 hours. Cell pellets were harvested and washed with ice-cold PBS. The nuclear and chromatin fractions were prepared as previously described (Mendez and Stillman, 2000). Equivalent fractions of proteins from the soluble nuclear extract and chromatin bound nuclear extract were resolved on SDS-PAGE and transferred on to PVDF membranes. The blots were probed with p53 (FL-393) and Histone H3 (marker for chromatin fraction) antibodies (Abcam, ab1791).

Immunofluorescent staining—TOV112D cells were treated with UCI-LC0023 or DMSO as a control for 3 hours on coverslips. Following treatments, the cells were fixed with 4% formaldehyde for 10 minutes at room temperature and permeabilized with 0.5% Triton X-100 for 5 minutes at room temperature. Cells were then blocked with buffer containing 4% horse serum and 0.1% gelatin for 40 minutes at 37°C. Cells were incubated with mouse PAB240 (EMD Millipore, OP-29) or mouse PAB1620 (EMD millipore, OP-33) that specifically recognizes the mutant or WT p53 respectively for overnight at 4°C. After three washes with 1% horse serum and 0.05% gelatin, cells were incubated with Alexa Fluor 488- conjugated donkey anti-mouse IgG (Invitrogen, A21202) at 37°C for 1 hour. Cells were stained with DAPI followed by overnight curing with Prolong Diamond Anti-Fade reagent (Invitrogen) in dark at room temperature. Cells were viewed with a Zeiss LSM 780 microscope and the fluorescent staining intensity was quantified using Volocity Software (Quorum Technologies).

Immunoprecipitation—TOV112D cells were pre-treated with 10μM Nutlin-3a (Sigma) for 6 hours followed by treatment with 30μM UCI-LC0023 or DMSO (Vehicle) for 3 hours. Cells were pelleted and suspended in lysis buffer containing 150mM NaCl, 50mM Tris-Cl pH −7.5, 10% Glycerol, 5mM EDTA and 1% NP-40. 90μg of lysate was diluted in lysis buffer and incubated overnight with PAB240 antibody at 4°C. Protein-G agarose beads (Fisher Scientific) were then added to the lysate and incubated for 2 hours at 4°C. The beads were washed three times with lysis buffer supplemented with protease inhibitors. Immunoprecipitants were eluted from the beads by boiling in Laemmli buffer at 95°C for 5 min and resolved on SDS-PAGE gels. The blots were probed with p53(FL-393) and GAPDH antibodies.

Chromatin Immunoprecipitation (ChIP)—TOV112D cells were treated with UCI-LC0023 or DMSO (Vehicle) for 30 minutes. Cells were fixed with 1% formaldehyde for 15 minutes at room temperature. Glycine was added to a final concentration of 0.125M and the cells were incubated for 10 minutes at room temperature. Cells were harvested and lysed in 500μl ice-cold cell lysis buffer (50 mM Tris/HCl [pH 8.0], 85 mM KCl, 0.5% NP40, 1 mM PMSF, 1 μg/ml pepstatin, 1 μg/ml leupeptin) for 10 minutes on ice. Cells were centrifuged at 3,000 rpm at 4°C for 5 min, and the precipitated nuclei were

resuspended in 500μl ice-cold RIPA buffer (50 mM Tris/ HCl [pH 8.0], 150 mM NaCl, 1 mM EDTA [pH 8.0], 1% Triton X-100, 0.1% SDS, 0.1% sodium deoxycholate,1 mM PMSF, 1 μg/ml pepstatin, 1 μg/ml leupeptin) and incubated on ice for 30 minutes. The samples were sonicated to fragment the DNA using Bioruptor® Pico (Diagenode). Samples were immunoprecipitated using clone DO-1 p53 antibody (Active Motif, 39553) along with no antibody control (mock) overnight at 4°C. Protein G agarose beads (Cell Signaling technology, 9007S) were added and samples were rocked for 3 hours at 4°C. The beads were washed and was subject to reverse-crosslinking in elution buffer overnight at 65°C. Input samples were handled identically. Next day, ChIP and Input samples were digested with 1 μg proteinase K and subsequently, DNA was purified by phenol/chloroform and resuspended in DNase free water.

RT-PCR was performed on a Biorad CFX Connect RT-PCR machine using the Biorad iTaq Universal SYBR Green SuperMix. Sequences of primers are:

p21-F: 5′-GTGGCTCTGATTGGCTTTCTG,

p21-R: 5′-CTGAAAACAGGCAGCCCAAGG;

PUMA-F: 5′-TCCTTGCCTTGGGCTAGGCC, and

PUMA-R: 5′-CGCGGACAAGTCAGGACTTG (Yu et al., 2012b)

Enrichment was calculated 2^-(ΔCt ChIP-ΔCt Input) and normalized to the no antibody control (mock).

RNA extraction, quantitative RT-PCR and NanoString analysis—TOV112D cells were treated with UCI-LC0023 or DMSO for 3 hours. RNA was extracted from cells using Qiagen RNeasy kit (Qiagen). cDNA was synthesized using Superscript reverse transcriptase III (Invitrogen). Gene expression levels were monitored by qRT-PCR using Biorad iTaq Universal SYBR Green SuperMix. The sequences of the primers used in qRT-PCR are:

p21-F: 5′- TGTCCGTCAGAACCCATGC-3’,

p21-R: 5′-AAAGTCGAAGTTCCATCGCTC-3’; (PrimerBank ID: 310832423c1)

NOXA -F: 5′- ACCAAGCCGGATTTGCGATT,

NOXA-R: 5′- ACTTGCACTTGTTCCTCGTGG; (PrimerBank ID: 21595743a1)

GAPDH -F: 5’- TCAACGACCACTTTGTCAAGCTCA and

GAPDH -R: 5’- GCTGGTGGTCCAGGG GTCTTACT

The gene expression level is normalized to GAPDH and the average is presented with S.D. from triplicates. For NanoString analysis, RNA samples from UCI-LC0023 treated and untreated TOV112D cells were run on custom-designed NanoString nCounter panel. The gene expression data was analyzed using nSolver software and the data is represented as log2 values of the mean.

Recombinant protein purification and DNA binding—Sequence corresponding to DNA-binding domain (DBD) of WT-p53 and $p53^{R175H}$ were cloned into modified pET28-smt3 vector with Ulp1-cleavage site following the smt3 tag. Each plasmid for protein expression in E. coli was transformed into Rosetta-BL21 (DE3). Protein expression was induced with 0.2 mM isopropyl-®-$_D$-1-thiogalactopyranoside (IPTG) for 16 h at 16°C. Cells were harvested at 5000 rpm for 10 min and disrupted by sonication on ice in lysis buffer (consisting of 25 mM Tris-HCl pH 8.0, 350 mM NaCl, 2 mM ®-mercaptoethanol, 2 mM Benzamidine, 1 mM PMSF, 30 mM Imidazole). The supernatant was applied onto Ni-NTA (Qiagen) using a peristaltic pump. After washing, the bound protein was eluted from the beads with elution buffer containing 300 mM imidazole. To remove the smt3 tag from the eluted proteins, Ulp1 was added in a 1:300 ratio (Ulp1: target) to eluted fractions before dialysis against 25 mM Tris-HCl pH 7.0, 70 mM NaCl, 2 mM DTT. After dialysis overnight at 4°C, each p53 protein was further purified by ion-exchange chromatography with a HiTrap Q-SP tandem system (GE Healthcare) to separate the target protein from nucleic acids, the smt3-tag, and Ulp1. p53 was eluted from the SP column with a gradient of NaCl. The eluted fractions were further purified by gel filtration chromatography (GE Healthcare). The purified protein was concentrated (~ 5 mg/ml) and stored at −80°C in storage buffer (consisting of 25 mM Tris-HCl pH 8.0, 350 mM NaCl, and 0.5 mM TCEP).

For *in vitro* DNA binding analysis, 5’ biotinylated DNA fragments representing the promoter of the p53-dependent *GADD45A* gene(El-Deiry et al., 1992) or a p53 non-consensus sequence (*E2F* consensus) were used. The sequences of 5’ biotinylated DNA fragments used are:

GADD45A-F:5′-TCGAGAGGCATGTCTAGGCATGTCTCTCGA-3’;

GADD45A-R:5′TCGAGAGACATGCCTAGACATGCCTCTCGA-3’

E2F-F:5’-TCGAGTTTCGCGCTTTCGCGCCTCGA-3’and

E2F- R: 5’-TCGAGGCGCGAAAGCGCGAAACTCGA-3’.

The annealed biotinylated DNA oligos (0.2μM) were incubated with Streptavidin beads (Thermo Scientific) in binding buffer (20mM HEPES [pH 7.9], 1mM $MgCl_2$, 1μM Zinc Acetate, 1μg/ml of Bovine Serum Albumin (BSA), 0.1%NP-40 and 1mM DTT) for 30 minutes at room temperature. Meanwhile, 100μM of UCI-LC0023 or DMSO was incubated separately with 0.2μM of purified DBD of $p53^{WT}$ or $p53^{R175H}$ protein in the binding buffer for 15 minutes at room temperature. The protein-drug mixture was added to the biotinylated DNA-bead mixture along with 200ng of Salmon sperm DNA and was incubated at room temperature for 2 hours. The beads were washed three times with binding buffer. Protein was eluted from the beads by boiling in Laemmli buffer at 95°C for 5 min and resolved on SDS-PAGE gels. The blots were probed with mouse PAB240 (OP-29, EMD Millipore).

Binding site mapping using Mass Spectrometry—Sequence corresponding to DNA-binding domain (DBD) of $p53^{R175H}$ was cloned into modified pET28-smt3 vector with Ulp1-cleavage site following the smt3 tag. Each plasmid was transformed into Rosetta-BL21 (DE3). Protein expression was induced with 0.2 mM isopropyl-®-$_D$-1-thiogalactopyranoside

(IPTG) for 16 h at 16°C. Cells were harvested at 5000 rpm for 10 min and disrupted by sonication on ice in lysis buffer (consisting of 25 mM Tris-HCl pH 8.0, 350 mM NaCl, 2 mM ®-mercaptoethanol, 2 mM Benzamidine, 1 mM PMSF, 30 mM Imidazole). 1mg of protein lysate was bound to Ni^{2+}-Sepharose beads (GE healthcare) at 4°C for 3 hours. Following three washes with lysis buffer, the beads were resuspended in binding buffer (20mM HEPES [pH 7.9], 1mM $MgCl_2$, 1μM Zinc Acetate, 1μg/ml of Bovine Serum Albumin (BSA), 0.1%NP-40 and 1mM DTT). The photo-cross linkable diazirine analog UCI-LC0045 was added to the beads and was incubated at room temperature for 15 minutes. Following incubation, the photo-cross linkable diazirine analog containing mixture was irradiated at 360nm at 4°C for 15 minutes. Control sample was treated in a similar way without UV activation.

The UV activated and control samples were resuspended in a buffer containing 8M Urea and 25 mM NH4HCO3. Proteins were reduced with 5mM DTT at 37°C for 15 minutes followed by reduction with 15mM iodoacetamide in the dark at room temperature for 30 minutes. The reaction was quenched with 5mM DTT for 30 minutes at room temperature. The proteins were then digested with trypsin (10ng/μl) at 37°C overnight in buffer containing 1.5M Urea and 25 mM NH4HCO3. The tryptic peptide mixtures were cleaned using OMIX C18 filter tips, evaporated to dryness using a SpeedVac vacuum concentrator, and resuspended in a buffer containing 2% formic acid and 3% ACN prior to LC-MS analysis.

The peptide mixtures were then analyzed by LC MS/MS using an UltiMate 3000 RSLC (Thermo Fisher) coupled to an Orbitrap Fusion Lumos mass spectrometer (Thermo Fisher). LC separation was performed on a 25 cm × 75 μm I.D. Acclaim® PepMap RSLC column. Peptides were eluted using a gradient of 4% to 25% B in 57 min at a flow rate of 300 nl/min (solvent A: 100% H2O, 0.1% formic acid; solvent B: 100% acetonitrile, 0.1% formic acid). Each MS cycle consisted of one survey scan measured in the Orbitrap (375–1500 m/z, 60k resolution) followed by 15 data-dependent MS/MS scans acquired in the ion trap with stepped-energy HCD (25±5% NCE). Raw spectrometric files were extracted to MGF format using MS Convert (Proteo Wizard) and searched using Batch-Tag within a developmental version (v. 6.0.0) of Protein Prospector at the University of California, San Francisco The mass accuracy for parent ions and fragment ions were set as ± 20 ppm and 0.6 Da, respectively. Trypsin was set as the enzyme, with a maximum of two missed cleavages allowed. Cysteine carbamidomethylation was set as a fixed modification, and protein N-terminal acetylation, methionine oxidation, and N-terminal conversion of glutamine to pyroglutamic acid were selected as variable modifications. In addition, a nonspecific modification corresponding to the mass of the UV-activated reagent (C20H18N2O2) was included as a variable modification.

Flow Cytometry—10^5 TOV-112D cells were seeded in 6-well plates. Cells were treated with 30μM UCI-LC0019 and UCI-LC0023, 40μM APR-246 or DMSO (Vehicle) and 1μM Doxorubicin (DOX). The cells were harvested and then incubated with Annexin V, Alexa Fluor™ 647 conjugate (Thermofisher, Cat# A23204), and Propidium Iodide PI (Sigma Aldrich, 25535164) for 5 minutes in Annexin-V Binding Buffer (10 mM HEPES (pH 7.5) 140 mM NaCl, and 2.5 mM $CaCl_2$) before FACS analyses using ACEA NovoCyte™ Flow Cytometer (Agilent Technologies, Inc., Santa Clara, CA).

Mouse Xenografts—Mice were housed and treated in accordance with approval of Institutional Animal Care and Use Committee (IACUC) from University of California, Irvine. Xenograft tumors were derived from injecting human tumor cell lines (3–5 × 10^6 cells/mice), TOV112D ($p53^{R175H}$), TOVII2D $^{p53-/-}$and HCT116 ($p53^{+/+}$). Tumors were allowed to grow to 50mm^3 prior to daily intraperitoneal injection of UCI-LC0019 (3.3 mg/kg or 10mg/kg). Tumor dimensions were measured every other day and their volumes were calculated by length (L) and width (W) by using the formula: volume = L × W^2 × 0.523. Corn oil was used as a delivery vehicle for UCI-LC0019. The number of mice used are: TOV112D (control – 10, treated – 9); TOVII2D $^{p53-/-}$ (control – 8, treated – 9) and HCT116 (control – 8, treated – 8). Tumor xenograft tissues fromTOV112D ($p53^{R175H}$) and TOVII2D $^{p53-/-}$ were stained with Clone DO-7 p53 antibody (Agilent Technologies, M7001) in accordance with the manufacturer's instructions.

GSH and LC0019 measurements using liquid chromatography mass spectrometry (LC-MS)—10mg of tumor tissues were extracted with 400μL of ice-cold acetonitrile:methanol:water (40:40:20) solution. Following vortexing and centrifugation at 16,000g for 10 min at 4 °C, 70μL of supernatant was loaded to MS vials. Metabolites were analyzed by quadrupole-orbitrap mass spectrometer (Q-Exactive Plus Hybrid Quadrupole-Orbitrap, Thermo Fisher) coupled to hydrophilic interaction chromatography (HILIC) via electrospray ionization. LC separation was on an Xbridge BEH amide column (2.1 mm × 150 mm, 2.5 μm particle size, 130 Å pore size; Waters) at 25°C using a gradient of solvent A (5% acetonitrile in water with 20 mM ammonium acetate and 20 mM ammonium hydroxide) and solvent B (100% acetonitrile). Flow rate was 150 μL/min. The LC gradient was: 0 min, 90% B; 2 min, 90% B; 3 min, 75% B; 7 min, 75% B; 8 min, 70% B; 9 min, 70% B; 10 min, 50% B; 12 min, 50% B; 13 min, 25% B; 14 min, 20% B; 15 min, 20% B; 16 min, 0% B; 20.5 min, 0% B; 21 min, 90% B; 25 min, 90% B. Autosampler temperature was set at 4°C and the injection volume of the sample was 3 μL. MS data were acquired in negative and positive ion mode with a full-scan mode from m/z 70 to 830 and 140,000 resolution. The identity of GSH and LC0019 were confirmed by MS^2 fragmentation and retention time with authentic chemical standards. Peaks that matched with GSH and LC0019 standards were identified with MAVEN software and Microsoft Excel was used for data presentation.

Compound synthesis—All chemicals were purchased from Sigma–Aldrich, Acros Organics, Alfa Aesar, TCI, Fisher Scientific, or CombiBlocks and used without further purification. Deuterated solvents were purchased from Cambridge Isotope Laboratories. Solvents were purchased as ACS grade or better and passed through a solvent purification system equipped with activated alumina columns prior to use. Unless otherwise stated, all reactions were performed in untreated glassware under ambient conditions. Reactions were monitored by thin layer chromatography (TLC) using glass plates coated with a 250 μm layer of 60 Å silica gel. TLC plates were visualized with a UV lamp at 254 nm, or by staining with potassium permanganate). Column chromatography was performed using forced flow (flash chromatography) on silica gel (SiO2) columns by standard techniques or with a Teledyne ISCO CombiFlash® on prepacked silica gel columns.

1H NMR spectra were recorded at 500 MHz or 600 MHz using either a Bruker DRX500 (cryoprobe) or Bruker AVANCE600 (cryoprobe) at 298.0 K. 13C{1H} NMR spectra were obtained at 125 MHz or 151 MHz on a Bruker DRX500 (cryoprobe) or Bruker AVANCE600 (cryoprobe) at 298.0 K. Chemical shifts (™) are reported in parts per million (ppm) and referenced to the residual solvent peak. NMR data are reported as follows: chemical shift, multiplicity (s = singlet, d = doublet, t = triplet, q = quartet, m = multiplet, dd = doublet of doublets, dt = doublet of triplets, triplet of triplets, ddd = doublet of doublet of doublets, app. = apparent, br = broad), coupling constants (J) in hertz (Hz), and integration. NMR spectra are reported in the Data S1 to S22 files.

General Procedure 1:

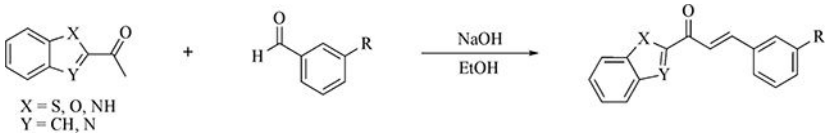

To a scintillation vial equipped with a magnetic stir bar the ketone (1 equiv.) and the aldehyde (1.1 equiv.) were dissolved in EtOH (0.5 M w.r.t. the ketone). NaOH (4 equiv.) was added as a 4 M aqueous solution. The reaction was then stirred for 24 hours. The reaction mixture was diluted with sat aq. NH4Cl (10 mL) and extracted with EtOAc (3 × 5 mL). The organic layers were combined, dried over Na2SO4, and concentrated to afford the yellow solids.

(*E*)-1-(benzo[*b*]thiophen-2-yl)-3-(*m*-tolyl)prop-2-en-1-one (UCI-LC0002)—

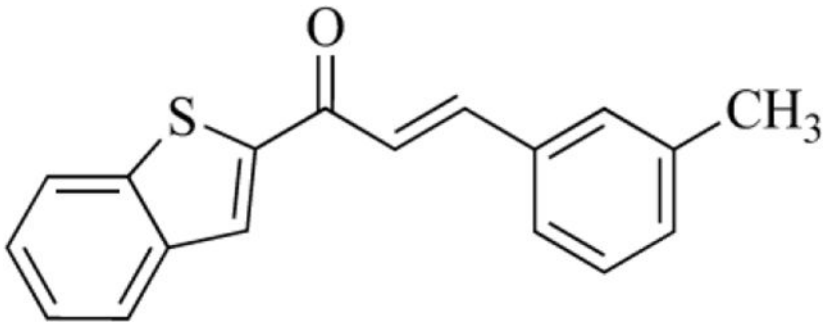

UCI-LC0002 was synthesized according to General Procedure 1. 4 M aq. NaOH (0.28 mL, 1.13 mmol) was added to 2-acetylbenzothiophene (50 mg, 0.28 mmol) and 3-methylbenzaldehyde (0.036 mL, 0.31 mmol) dissolved in EtOH (0.57 mL). UCI-LC0002 was recrystallized from EtOH affording a yellow powder 3 mg (4% yield). 1H NMR (500 MHz, CDCl3) δ 8.13 (s, 1H), 7.93 (m, 1H), 7.91 (m, 1H), 7.88 (d, J = 15.6 Hz, 1H), 7.54 (d, J = 15.6 Hz, 1H), 7.51 – 7.46 (m, 3H), 7.45 – 7.41 (m, 1H), 7.34 (m, 1H), 7.27–7.25 (m, J = 7.8 Hz, 1H), 2.42 (s, 3H); 13C{1H} NMR (125 MHz, CDCl3) δ 183.6, 145.4, 144.8, 142.8, 139.4, 138.8 134.7, 131.8, 129.3, 129.0, 128.9, 127.5, 126.1, 126.0, 125.2, 123.2, 121.0, 21.5 (Data S1).

(*E*)-1-(benzo[*b*]thiophen-2-yl)-3-(3-nitrophenyl)prop-2-en-1-one (UCI-LC0003)—

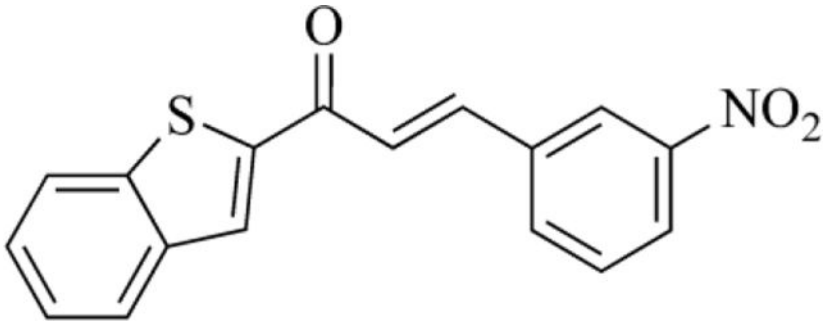

UCI-LC0003 was synthesized according to General Procedure 1. 4 M aq. NaOH (0.28 mL, 1.13 mmol) was added to 2-acetylbenzothiophene (50 mg, 0.28 mmol) and 3-nitrobenzaldehyde (47 mg, 0.31 mmol) dissolved in EtOH (0.57 mL). UCI-LC0003 was recrystallized from EtOH affording an off-white solid 8 mg (9% yield). 1H NMR (500 MHz, CDCl3) δ 8.57 (s, 1H), 8.29 (m, 1H), 8.19 (s, 1H), 7.99–7.88 (m, 4H), 7.67 (d, J = 15.5 Hz, 1H), 7.65 (t, J = 8.0 Hz, 1H), 7.51 (m, 1H), 7.45 (t, J = 7.5 Hz, 1H); 13C{1H} NMR (125 MHz, CDCl3) δ 182.9, 144.8, 143.1, 141.4, 139.3, 136.5, 134.8, 130.3, 129.7, 128.0, 126.3, 125.4, 125.0, 123.8, 123.2, 122.4, 110.1 (Data S2).

(*E*)-1-(benzo[*b*]thiophen-2-yl)-3-phenylprop-2-en-1-one (UCI-LC0005)—

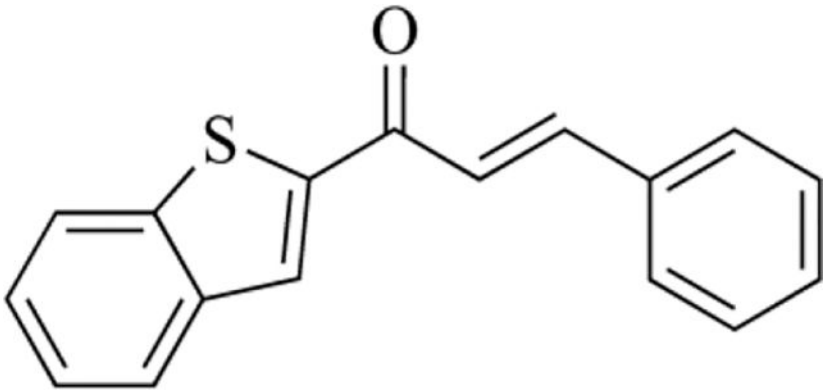

UCI-LC0005 was synthesized according to General Procedure 1. 4 M aq. NaOH (0.28 mL, 1.13 mmol) was added to 2-acetylbenzothiophene (50 mg, 0.28 mmol) and benzaldehyde (0.032 mL, 0.31 mmol) dissolved in EtOH (0.57 mL). UCI-LC0005 was recrystallized from EtOH affording a yellow powder 22 mg (30% yield). 1H NMR (500 MHz, CDCl3) δ 8.11 (s, 1H), 7.94–7.88 (m, 3H), 7.70–7.67 (m, 2H), 7.55 (d, J = 15.6 Hz, 1H), 7.48 (ddd, J = 8.2, 7.1, 1.3 Hz, 1H), 7.46–7.41 (m, 4H); 13C{1H} NMR (125 MHz, CDCl3) δ 183.5, 145.3, 144.5, 142.8, 139.4, 134.7, 130.9, 129.1, 129.0, 128.7, 127.6, 126.1, 125.2, 123.1, 121.2 (Data S3).

(*E*)-1-(benzo[*b*]thiophen-2-yl)-3-(3-methoxyphenyl)prop-2-en-1-one (UCI-LC0006)—

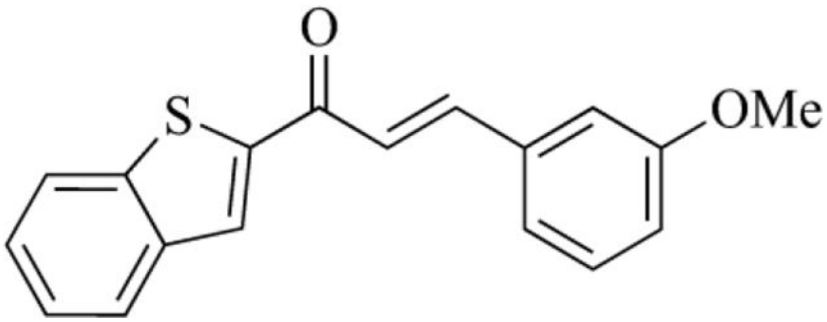

UCI-LC0006 was synthesized according to General Procedure 1. 4 M aq. NaOH (0.28 mL, 1.13 mmol) was added to 2-acetylbenzothiophene (50 mg, 0.28 mmol) and 3-methoxybenzaldehyde (0.038 mL, 0.31 mmol) dissolved in EtOH (0.57 mL). UCI-LC0006 was recrystallized from EtOH affording a yellow powder 31 mg (38% yield). 1H NMR (500 MHz, CDCl3) δ 8.10 (s, 1H), 7.92 (d, J = 8.0 Hz, 1H), 7.89 (d, J = 8.1 Hz, 1H), 7.85 (d, J = 15.6 Hz, 1H), 7.52 (d, J = 15.6 Hz, 1H), 7.47 (ddd, J = 8.1, 7.1, 1.3 Hz, 1H), 7.42 (ddd, J = 8.0, 7.1, 1.2 Hz, 1H), 7.35 (t, J = 7.9 Hz, 1H), 7.27 (d, J = 7.9 Hz, 1H), 7.19–7.17 (m, 1H), 7.00–6.98 (m, 1H), 3.87 (s, 3H) ; 13C{1H} NMR (125 MHz, CDCl3) δ 183.5, 160.1, 145.3, 144.4, 142.8, 139.4, 136.1, 130.1, 129.0, 127.6, 126.1, 125.2, 123.1, 121.4, 121.3, 116.6, 113.7, 55.5 (Data S4).

(*E*)-1-(benzo[*b*]thiophen-2-yl)-3-(3-bromophenyl)prop-2-en-1-one (UCI-LC0008)—

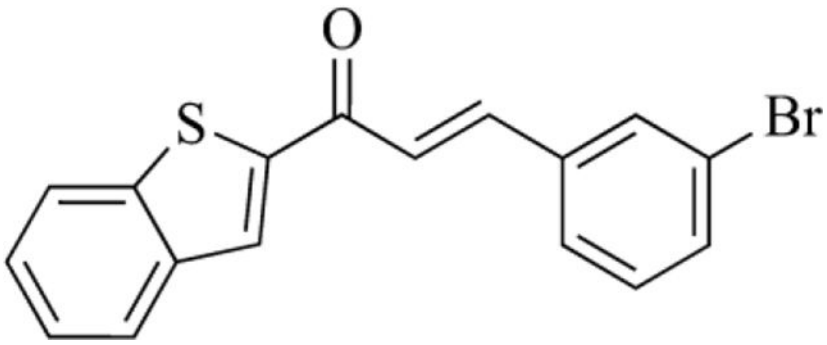

UCI-LC0008 was synthesized according to General Procedure 1. 4 M aq. NaOH (0.28 mL, 1.13 mmol) was added to 2-acetylbenzothiophene (50 mg, 0.28 mmol) and 3-bromobenzaldehyde (0.036 mL, 0.31 mmol) dissolved in EtOH (0.57 mL). **UCI-LC0008** was recrystallized from EtOH affording a yellow powder 11 mg (11% yield). **^{1}H NMR** (500 MHz, $CDCl_3$) δ 8.13 (s, 1H), 7.94 (m, 1H), 7.90 (d, *J* = 8.1 Hz, 1H), 7.83 (t, *J* = 1.9 Hz, 1H), 7.79 (d, *J* = 15.6 Hz, 1H), 7.58–7.54 (m, 2H), 7.52 (d, *J* = 15.6 Hz, 1H), 7.49 (ddd, *J* = 8.2, 7.0, 1.3 Hz, 1H), 7.43 (ddd, *J* = 8.1, 7.1, 1.2 Hz, 1H), 7.31 (t, *J* = 7.8 Hz, 1H); **^{13}C{1H} NMR** (125 MHz, $CDCl_3$) δ 183.2, 145.0, 142.9, 142.6, 139.3, 136.9, 133.6, 131.0, 130.7, 129.3, 127.7, 127.6, 126.2, 125.3, 123.3, 123.2, 122.4 (Data S5).

(*E*)-1-(benzofuran-2-yl)-3-phenylprop-2-en-1-one (UCI-LC0009)—

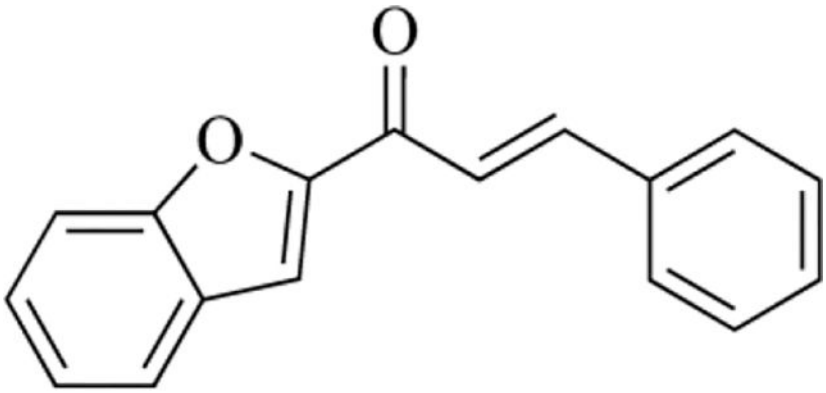

UCI-LC0009 was synthesized according to General Procedure 1. 4 M aq. NaOH (0.31 mL, 1.25 mmol) was added to 2-acetylbenzofuran (50 mg, 0.31 mmol) and benzaldehyde (0.035 mL, 0.34 mmol) dissolved in EtOH (0.62 mL). **UCI-LC0009** was recrystallized from EtOH affording an off-white solid 10 mg (13% yield). **^{1}H NMR** (500 MHz, $CDCl_3$) δ 7.96 (d, *J* = 15.7 Hz, 1H), 7.75 (dd, J = 7.8, 1.0 Hz, 1H), 7.72–7.69 (m, 2H), 7.66 (d, *J* = 1.0 Hz, 1H), 7.64 (dd, *J* = 8.4, 1.0 Hz, 1H), 7.61 (d, *J* = 15.7 Hz, 1H), 7.50 (ddd, *J* = 8.4, 7.2, 1.3 Hz, 1H), 7.46–7.43 (m, 3H), 7.34 (m, 1H); **^{13}C{1H} NMR** (125 MHz, $CDCl_3$) δ 179.9, 155.9, 153.8, 144.8, 134.7, 131.0, 129.1, 128.8, 128.4, 127.4, 124.1, 123.4, 121.2, 113.4, 112.6 (Data S6).

(*E*)-1-(benzofuran-2-yl)-3-(3-methoxyphenyl)prop-2-en-1-one (UCI-LC0010)—

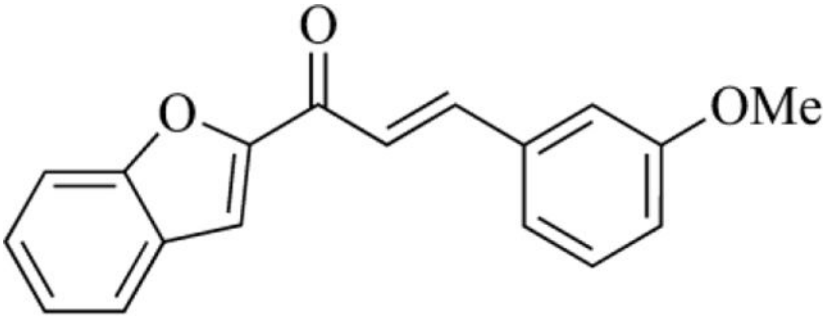

UCI-LC0010 was synthesized according to General Procedure 1. 4 M aq. NaOH (0.31 mL, 1.25 mmol) was added to 2-acetylbenzofuran (50 mg, 0.31 mmol) and 3-methoxybenzaldehyde (0.042 mL, 0.34 mmol) dissolved in EtOH (0.62 mL). **UCI-LC0010** was recrystallized from EtOH affording an off-white solid 9 mg (10% yield). **^{1}H NMR** (500 MHz, $CDCl_3$) δ 7.92 (d, *J* = 15.7 Hz, 1H), 7.74 (m, 1H), 7.66 (d, *J* = 1.0 Hz, 1H), 7.64 (dd, *J* = 8.4, 0.9, Hz 1H), 7.58 (d, *J* = 15.7 Hz, 1H), 7.50 (ddd, *J* = 8.4, 7.2, 1.2 Hz, 1H), 7.36 (t, *J* = 7.8 Hz, 1H), 7.34 (ddd, *J* = 8.0, 7.2, 0.9 Hz, 1H), 7.31–7.29 (m, 1H), 7.21–7.20 (m 1H), 6.99 (ddd, *J* = 8.2, 2.6, 1.0 Hz, 1H), 3.88 (s, 3H); **^{13}C{1H} NMR** (125 MHz, $CDCl_3$) δ 179.8, 160.1, 155.9, 153.8, 144.7, 136.1, 130.1, 128.4, 127.4, 124.1, 123.4, 121.513, 121.506, 116.8, 113.8, 113.4, 112.6, 55.5 (Data S7).

(*E*)-1-(1*H*-indol-2-yl)-3-phenylprop-2-en-1-one (UCI-LC0012)—

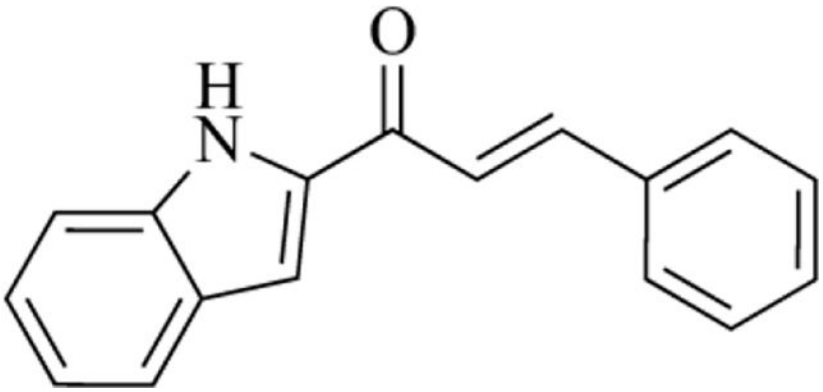

UCI-LC0012 was synthesized according to General Procedure 1. 4 M aq. NaOH (0.31 mL, 1.26 mmol) was added to 2-acetylindole (50 mg, 0.31 mmol) and benzaldehyde (0.035 mL, 0.35 mmol) dissolved in EtOH (0.63 mL). **UCI-LC0012** was isolated as a yellow powder after silica gel column chromatography (15% EtOAc/hexanes) to afford 27 mg (35% yield). **^{1}H NMR** (500 MHz, DMSO–d_6) δ 11.84 (brs, 1H), 7.89 (d, *J* = 15.7 Hz, 1H), 7.88–7.86 (m, 2H), 7.75–7.73 (m, 1H), 7.73 (d, *J* = 15.7 Hz, 1H), 7.69 (dd, *J* = 8.1, 1.1 Hz, 1H), 7.46–7.41 (m, 4H), 7.26 (ddd, *J* = 8.2, 6.9, 1.1 Hz, 1H), 7.06 (ddd, *J* = 8.0, 6.9, 1.0 Hz, 1H); **^{13}C{1H} NMR** (125 MHz, DMSO–d_6) δ 180.6, 142.0, 138.3, 136.8, 134.7, 130.4, 128.9, 128.8, 127.1, 125.7, 122.8, 122.6, 120.3, 112.7, 110.0 (Data S8).

(*E*)-1-(1*H*-indol-2-yl)-3-(3-methoxyphenyl)prop-2-en-1-one (UCI-LC0013)—

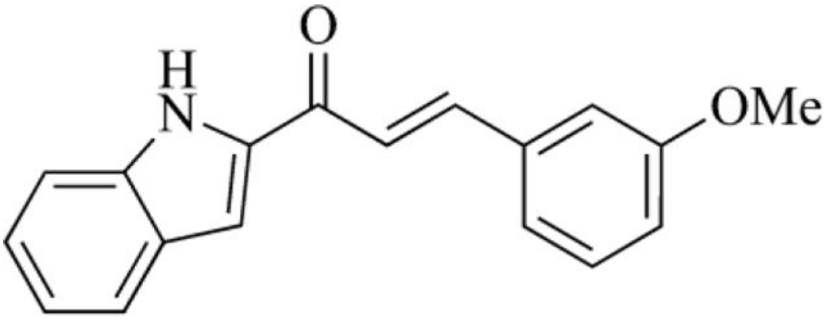

UCI-LC0013 was synthesized according to General Procedure 1. 4 M aq. NaOH (0.31 mL, 1.26 mmol) was added to 2-acetylindole (50 mg, 0.31 mmol) and 3-methoxybenzaldehyde (0.043 mL, 0.35 mmol) dissolved in EtOH (0.63 mL). **UCI-LC0013** was isolated as a yellow powder after silica gel column chromatography (15% EtOAc/hexanes) to afford 13 mg (15% yield). **^{1}H NMR** (500 MHz, K_2CO_3 buffered $CDCl_3$) δ 9.27 (brs, 1H), 7.88 (d, *J* = 15.6 Hz, 1H), 7.76 (dt, *J* = 8.1, 1.0 Hz, 1H), 7.51 (d, *J* = 15.6 Hz, 1H), 7.46 (dt, *J* = 8.4, 0.9 Hz, 1H), 7.39–7.35 (m, 3H), 7.29 (m, 1H), 7.20–7.16 (m, 2H), 6.99 (ddd, *J* = 8.2, 2.6, 1.0 Hz, 1H), 3.88 (s, 3H); **^{13}C{1H} NMR** (125 MHz, K_2CO_3 buffered $CDCl_3$) δ 181.2, 160.1, 143.4, 137.8, 136.6, 136.3, 130.1, 128.0, 126.7, 123.3, 121.9, 121.3, 121.2, 116.5, 113.7, 112.3, 109.6, 55.5 (Data S9).

(*E*)-3-(3-bromophenyl)-1-(1*H*-indol-2-yl)prop-2-en-1-one (UCI-LC0014)—

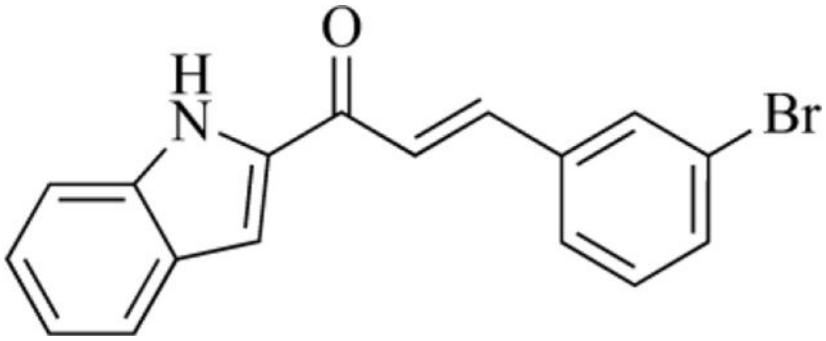

UCI-LC0014 was synthesized according to General Procedure 1. 4 M aq. NaOH (1.57 mL, 6.28 mmol) was added to 2-acetylindole (250 mg, 1.57 mmol) and 3-bromobenzaldehyde (0.20 mL, 1.73 mmol) dissolved in EtOH (3.14 mL). **UCI-LC0014** was isolated as a yellow powder after silica gel column chromatography (1% MeOH/CH_2Cl_2) to afford 150 mg (29% yield). **^{1}H NMR** (500 MHz, K_2CO_3 buffered $CDCl_3$) δ 9.26 (brs, 1H), 7.83 (s, 1H), 7.82 (d, *J* = 15.9 Hz, 1H), 7.76 (d, *J* = 8.1 Hz, 1H), 7.58 (d, *J* = 7.8 Hz, 1H), 7.55 (d, *J* = 8.0 Hz, 1H), 7.50 (d, *J* = 15.7 Hz, 1H), 7.46 (d, *J* = 8.3 Hz, 1H), 7.40 (s, 1H), 7.38 (t, *J* = 8.0 Hz, 1H) 7.32 (t, *J* = 8.0 Hz, 1H), 7.18 (t, *J* = 7.5 Hz, 1H); **^{13}C{1H} NMR** (125 MHz, K_2CO_3 buffered $CDCl_3$) δ 180.8, 141.6, 137.9, 137.1, 136.5, 133.4 131.0, 130.6, 127.9, 127.5, 126.9, 123.4, 123.3, 122.9, 121.3, 112.3, 109.9 (Data S10).

(*E*)-3-(3-fluorophenyl)-1-(1*H*-indol-2-yl)prop-2-en-1-one (UCI-LC0015)—

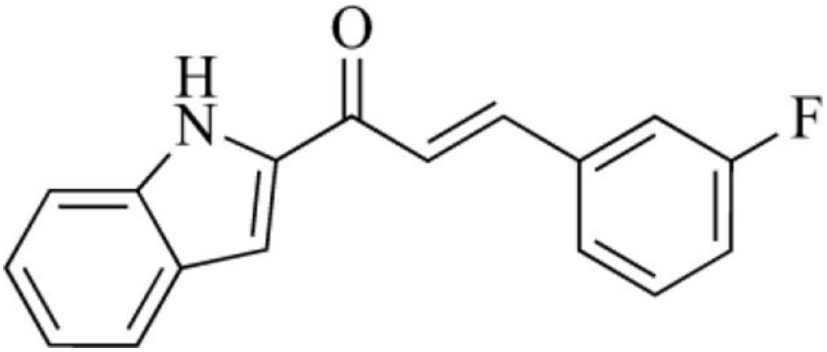

UCI-LC0015 was synthesized according to General Procedure 1. 4 M aq. NaOH (0.31 mL, 1.26 mmol) was added to 2-acetylindole (50 mg, 0.31 mmol) and 3-fluorobenzaldehyde (0.037 mL, 0.35 mmol) dissolved in EtOH (0.63 mL). **UCI-LC0015** was isolated as a yellow clumpy solid after silica gel column chromatography (15% EtOAc/hexanes) to afford 26 mg (31% yield). **^{1}H NMR** (500 MHz, K_2CO_3 buffered $CDCl_3$) δ 9.28 (brs, 1H), 7.86 (d, *J* = 15.7 Hz, 1H), 7.76 (dt, *J* = 8.1, 0.9 Hz, 1H), 7.51 (d, *J* = 15.7 Hz, 1H), 7.47–7.37 (m, 5H), 7.20–7.17 (m, 1H), 7.13 (tt, *J* = 8.0, 2.1 Hz, 1H); **^{13}C{1H} NMR** (125 MHz, K_2CO_3 buffered $CDCl_3$) δ 180.9, 163.2 (d, $^1J_{C,F}$ = 247.0 Hz), 141.9 (d, $^4J_{C,F}$ = 2.6 Hz), 137.9, 137.2 (d, $^3J_{C,F}$ = 7.8 Hz), 136.5, 130.7 (d, $^3J_{C,F}$ = 8.3 Hz), 127.9, 126.9, 124.7 (d, $^4J_{C,F}$ = 2.9 Hz), 123.4, 122.9, 121.3, 117.5 (d, $^2J_{C,F}$ = 21.5 Hz), 114.7 (d, $^2J_{C,F}$ = 21.8 Hz), 112.3, 109.9 (Data S11).

(*E*)-1-(1*H*-indol-2-yl)-3-(3-(trifluoromethyl)phenyl)prop-2-en-1-one (UCI-LC0016)—

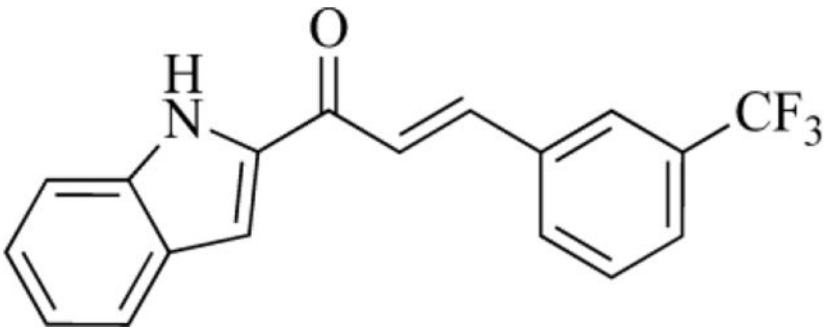

UCI-LC0016 was synthesized according to General Procedure 1. 4 M aq. NaOH (0.31 mL, 1.26 mmol) was added to 2-acetylindole (50 mg, 0.31 mmol) and 3-trifluoromethylbenzaldehyde (0.047 mL, 0.35 mmol) dissolved in EtOH (0.63 mL). **UCI-LC0016** was isolated as a fluffy yellow solid after silica gel column chromatography (15% EtOAc/hexanes) to afford 24 mg (24% yield). **^{1}H NMR** (500 MHz, DMSO–d_6) δ 11.92 (brs, 1H), 8.36 (s, 1H), 8.20 (d, J = 7.8 Hz, 1H), 8.10 (d, J = 15.7 Hz, 1H), 7.88 (s, 1H), 7.85 (d, J = 15.7 Hz, 1H), 7.80 (d, J = 7.9 Hz, 1H), 7.74 (d, J = 8.1 Hz, 1H), 7.71 (t, J = 7.8 Hz, 1H), 7.49 (d, J = 8.3, 1H), 7.32 (m, 1H), 7.11 (t, J = 7.5 Hz, 1H); **^{13}C{1H} NMR** (125 MHz, DMSO–d_6) δ 180.5, 140.2, 138.4, 136.8, 135.9, 132.8, 129.9, 129.8 (q, $^{2}J_{C,F}$ = 31.7 Hz), 127.1, 126.5 (q, $^{3}J_{C,F}$ = 3.7 Hz), 125.9, 125.0 (q, $^{3}J_{C,F}$ = 3.8 Hz), 124.5, 124.1 (q, $^{1}J_{C,F}$ = 272.6 Hz), 122.8, 120.4, 112.8, 110.6 (Data S12).

(*E*)-1-(1*H*-indol-2-yl)-3-(3-nitrophenyl)prop-2-en-1-one (UCI-LC0018)—

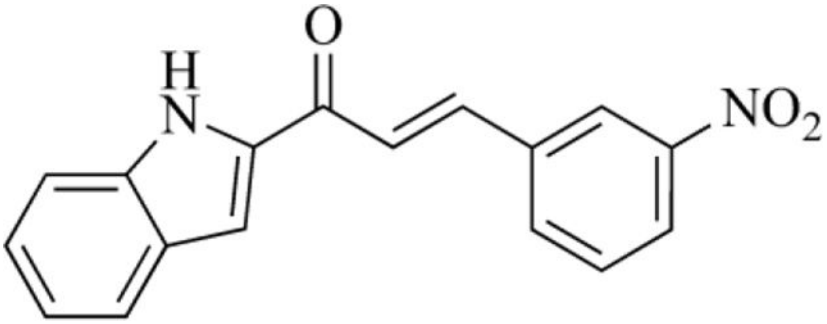

UCI-LC0018 was synthesized according to General Procedure 1. 4 M aq. NaOH (0.31 mL, 1.26 mmol) was added to 2-acetylindole (50 mg, 0.31 mmol) and 3-nitrobenzaldehyde (53 mg, 0.35 mmol) dissolved in EtOH (0.63 mL). **UCI-LC0018** was isolated as a yellow powder after silica gel column chromatography (15% EtOAc/hexanes) to afford 43 mg (47% yield). **^{1}H NMR** (500 MHz, DMSO–d_6) δ 11.93 (brs, 1H), 8.80 (s, 1H), 8.36 (d, J = 7.7 Hz, 1H), 8.27 (m, 1H), 8.14 (d, J = 15.7 Hz, 1H), 7.90 (s, 1H), 7.89 (d, J = 15.7 Hz, 1H), 7.76 (t, J = 7.9 Hz, 1H), 7.75 (d, J = 8.3 Hz, 1H), 7.49 (t, J = 8.3 Hz, 1H), 7.32 (m, 1H), 7.11 (t, J = 7.5 Hz, 1H); **^{13}C{1H} NMR** (125 MHz, DMSO–d_6) δ 180.4, 148.5, 139.5, 138.4, 136.7, 136.6, 135.0, 130.3, 127.1, 125.9, 125.3, 124.5, 122.85, 122.84 120.4, 112.8, 110.8 (Data S13).

(*E*)-1-(1*H*-benzo[*d*]imidazol-2-yl)-3-(3-methoxyphenyl)prop-2-en-1-one (UCI-LC0019)—

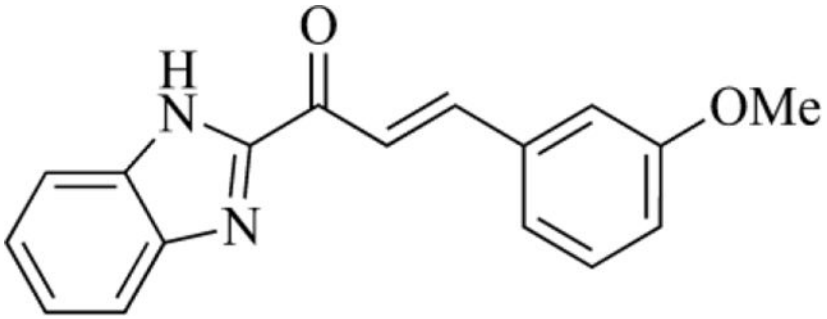

UCI-LC0019 was synthesized according to General Procedure 1. 4 M aq. NaOH (0.31 mL, 1.25 mmol) was added to 1-(1*H*-benzo[*d*]imidazol-2-yl)ethan-1-one (50 mg, 0.31 mmol) and 3-methoxybenzaldehyde (0.041 mL, 0.34 mmol) dissolved in EtOH (0.62 mL). **UCI-LC0019** was isolated as a yellow powder after silica gel column chromatography (15% EtOAc/hexanes) to afford 62 mg (71% yield). **^{1}H NMR** (500 MHz, K_2CO_3 buffered $CDCl_3$) δ 11.02 (brs, 1H), 8.13 (d, *J* = 15.9 Hz, 1H), 8.05 (d, *J* = 16.0 Hz, 1H), 7.95 (d, *J* = 8.1 Hz, 1H), 7.58 (d, *J* = 8.0 Hz, 1H), 7.43 (t, *J* = 7.5 Hz, 1H), 7.39 – 7.35 (m, 1H), 7.33 (m, 2H), 7.26 (s, 1H), 6.99 (m, 1H), 3.85 (s, 3H); **^{13}C{1H} NMR** (125 MHz, K_2CO_3 buffered $CDCl_3$) δ 181.8, 160.1, 149.0, 146.2, 143.8, 136.0, 134.1, 130.1, 126.7, 124.0, 122.3, 122.0, 121.3, 117.7, 113.5, 112.4, 55.6 (Data S14 and S15).

(*E*)-1-(1*H*-benzo[*d*]imidazol-2-yl)-3-phenylprop-2-en-1-one (UCI-LC0020)—

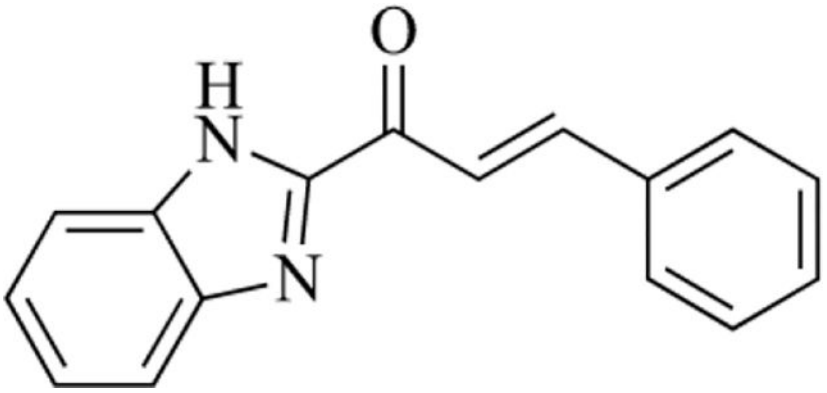

UCI-LC0020 was synthesized according to General Procedure 1. 4 M aq. NaOH (0.31 mL, 1.25 mmol) was added to 1-(1*H*-benzo[*d*]imidazol-2-yl)ethan-1-one (50 mg, 0.31 mmol) and benzaldehyde (0.035 mL, 0.34 mmol) dissolved in EtOH (0.62 mL). **UCI-LC0020** was isolated as an off-white solid after silica gel column chromatography (20% EtOAc/hexanes) to afford 28 mg (36% yield). **^{1}H NMR** (500 MHz, K_2CO_3 buffered $CDCl_3$) δ 10.57 (brs, 1H), 8.15 (d, *J* = 16.0 Hz, 1H), 8.09 (d, *J* = 16.0 Hz, 1H), 7.97 (d, *J* = 8.2 Hz, 1H), 7.78–7.76 (m, 2H), 7.59 (d, *J* = 8.1 Hz, 1H), 7.46–7.43 (m, 4H), 7.39 (ddd, *J* = 8.3, 7.1, 1.2 Hz, 1H); **^{13}C{1H} NMR** (125 MHz, K_2CO_3 buffered $CDCl_3$) δ 181.6, 149.0, 146.2, 143.9, 134.7, 133.9, 131.3, 129.3, 129.1, 126.7, 124.0, 122.2, 121.1, 112.2 (Data S16).

(*E*)-1-(1*H*-benzo[*d*]imidazol-2-yl)-3-(3-fluorophenyl)prop-2-en-1-one (UCI-LC0021)—

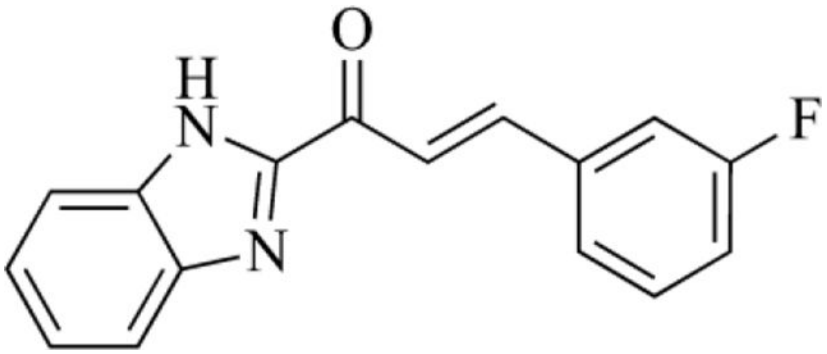

UCI-LC0021 was synthesized according to General Procedure 1. 4 M aq. NaOH (0.31 mL, 1.25 mmol) was added to 1-(1*H*-benzo[*d*]imidazol-2-yl)ethan-1-one (50 mg, 0.31 mmol) and 3-fluorobenzaldehyde (0.036 mL, 0.34 mmol) dissolved in EtOH (0.62 mL). **UCI-LC0021** was isolated as a fluffy yellow solid after silica gel column chromatography (20% EtOAc/hexanes) to afford 21 mg (25% yield). **^{1}H NMR** (500 MHz, DMSO–d_6) δ 13.51 (brs, 1H), 8.14 (d, J = 16.1 Hz, 1H), 7.97 (d, J = 16.1 Hz, 1H), 7.87 (d, J = 8.1 Hz, 1H), 7.75 (m, 1H), 7.73 (d, J = 7.8, Hz 1H), 7.59 (d, J = 8.1 Hz, 1H), 7.53 (m, 1H), 7.41 (t, J = 7.5 Hz, 1H), 7.35–7.31 (m, 2H); **^{13}C{1H} NMR** (125 MHz, DMSO–d_6) δ 180.9, 162.5 (d, $^{1}J_{C,F}$ = 244.3 Hz), 148.8, 143.0, 142.8 (d, $^{4}J_{C,F}$ = 2.5 Hz), 136.8 (d, $^{3}J_{C,F}$ = 8.0 Hz), 134.8, 131.0 (d, $^{3}J_{C,F}$ = 8.3 Hz), 125.8, 125.1 (d, $^{4}J_{C,F}$ = 2.6 Hz), 123.2, 123.0, 121.2, 117.7 (d, $^{2}J_{C,F}$ = 21.3 Hz), 115.2 (d, $^{2}J_{C,F}$ = 22.0 Hz), 112.9 (Data S17).

(*E*)-1-(1*H*-benzo[*d*]imidazol-2-yl)-3-(3-(trifluoromethyl)phenyl)prop-2-en-1-one (UCI-LC0022)—

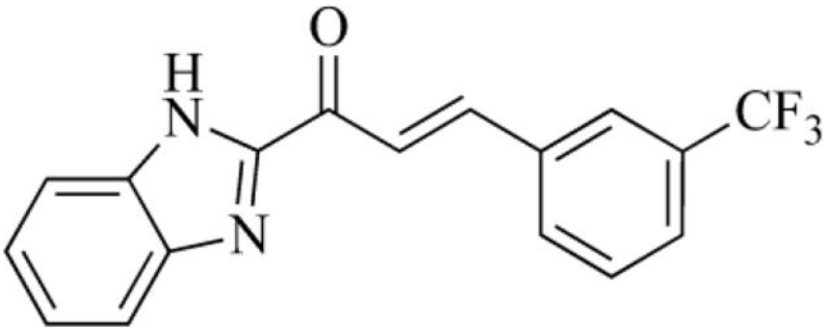

UCI-LC0022 was synthesized according to General Procedure 1. 4 M aq. NaOH (0.31 mL, 1.25 mmol) was added to 1-(1*H*-benzo[*d*]imidazol-2-yl)ethan-1-one (50 mg, 0.31 mmol) and 3-trifluoromethylbenzaldehyde (0.046 mL, 0.34 mmol) dissolved in EtOH (0.62 mL). **UCI-LC0022** was isolated as a tan powder after silica gel column chromatography (20–40% EtOAc/hexanes) to afford 59 mg (60% yield). **^{1}H NMR** (500 MHz, DMSO–d_6) δ 13.53 (brs, 1H), 8.23 (d, J = 16.1 Hz, 1H), 8.24–8.20 (m, 2H), 8.06 (d, J = 16.2 Hz, 1H), 7.84 (d, J = 7.8 Hz, 1H), 7.77–7.69 (m, 3H), 7.40–7.36 (m, 2H); **^{13}C{1H} NMR*** (125 MHz, DMSO–d_6) δ 180.9, 148.8, 142.3, 135.5, 132.3, 130.2, 129.9 (q, $^{2}J_{C,F}$ = 31.8 Hz), 127.1 (q, $^{3}J_{C,F}$ = 3.6 Hz), 125.d (q, $^{3}J_{C,F}$ = 3.8 Hz), 124 (q, $^{1}J_{C,F}$ = 272.8 Hz), 123.5 (Data S18).

* DMSO–d_6 was used instead of K_2CO_3 buffered $CDCl_3$ due to the poor solubility of the substrate in chloroform. Sridharan and coworkers suggested that the presence of DMSO–d_6 could interrupt the intramolecular hydrogen bonding event between the benzimidazole N–H and the hydroxy oxygen of 2-(2-hydroxy-5-substituted-aryl) benzimidazoles (shown below) (Sridharan et al., 2005). At higher concentrations, intermolecular hydrogen bonding between the benzimidazole substrate and the NMR solvent appeared to predominate. Consequently, certain ^{13}C NMR signals for some of the tested substrates were noted to not be visible (3a, 4, 7, and 7a) or were observed to merge with those of the cumyl group (5 and 6). It is suspected that this disruption of intramolecular hydrogen bonding between the benzimidazole nitrogen and the ketone in **UCI-LC0022, UCI-LC0023, and enone A** is the reason why the ^{13}C NMR demonstrates exhibits 6 less resonances than expected in DMSO–d_6.

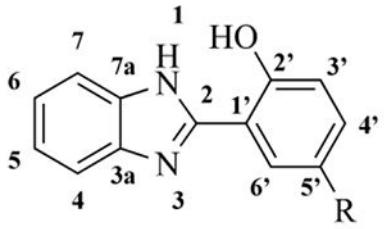

2-(2-hydroxy-5-substituted-aryl) benzimidazole

(*E*)-1-(1*H*-benzo[*d*]imidazol-2-yl)-3-(3-nitrophenyl)prop-2-en-1-one (UCI-LC0023)—

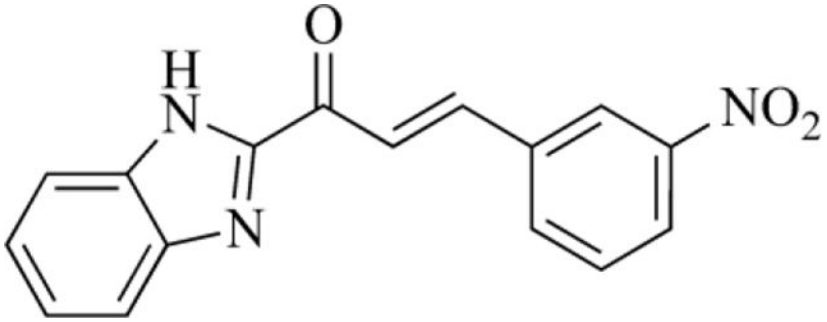

UCI-LC0023 was synthesized according to General Procedure 1. 4 M aq. NaOH (0.31 mL, 1.25 mmol) was added to 1-(1*H*-benzo[*d*]imidazol-2-yl)ethan-1-one (50 mg, 0.31 mmol) and 3-nitrobenzaldehyde (51 mg, 0.34 mmol) dissolved in EtOH (0.62 mL). **UCI-LC0023** was isolated as a yellow powder after silica gel column chromatography (30–40% EtOAc/hexanes) to afford 26 mg (28% yield). **^{1}H NMR** (500 MHz, DMSO–d_6) δ 13.54 (brs, 1H), 8.67 (s, 1H), 8.36 (d, J = 7.7 Hz, 1H), 8.31 (m, 1H), 8.26 (d, J = 16.2 Hz, 1H), 8.09 (d, J = 16.2 Hz, 1H), 7.97–7.82 (m, 1H), 7.77 (t, J = 8.0 Hz, 1H), 7.67–7.53 (m, 1H), 7.46–7.32 (m, 2H); **^{13}C{1H} NMR*** (125 MHz, DMSO–d_6) δ 180.8, 148.7, 148.4, 141.6, 136.1, 134.7, 130.6, 125.1, 124.2 123.3 (Data S19).

(*E*)-1-(1*H*-benzo[*d*]imidazol-2-yl)-3-(*m*-tolyl)prop-2-en-1-one (UCI-LC0024)—

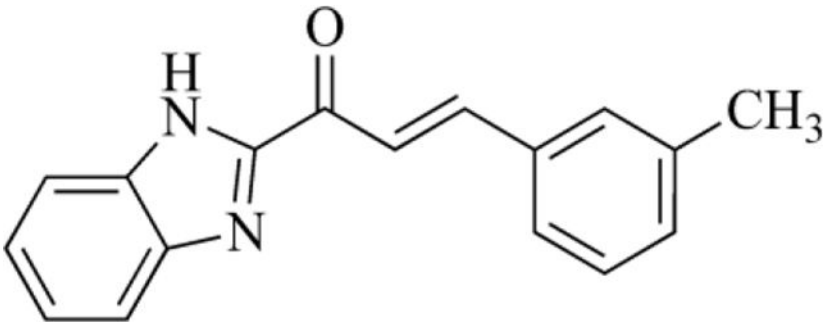

UCI-LC0024 was synthesized according to General Procedure 1. 4 M aq. NaOH (0.31 mL, 1.25 mmol) was added to 1-(1*H*-benzo[*d*]imidazol-2-yl)ethan-1-one (50 mg, 0.31 mmol) and 3-methylbenzaldehyde (0.040 mL, 0.34 mmol) dissolved in EtOH (0.62 mL). **UCI-LC0024** was isolated as a yellow powder after silica gel column chromatography (20% EtOAc/hexanes) to afford 30 mg (37% yield). **^{1}H NMR** (500 MHz, K_2CO_3 buffered $CDCl_3$) δ 10.54 (br s, 1H), 8.13 (d, *J* = 16.0 Hz, 1H), 8.06 (d, *J* = 16.0 Hz, 1H), 7.97 (d, *J* = 8.1 Hz, 1H), 7.61 (s, 1H), 7.59 (d, *J* = 8.1 Hz, 1H), 7.55 (d, *J* = 7.6 Hz, 1H), 7.46–7.43 (m, 1H), 7.40–7.37 (m, 1H), 7.33 (t, *J* = 7.6 Hz, 1H), 7.28–7.25 (m, 1H), 2.41 (s, 3H); **^{13}C{1H} NMR** (125 MHz, K_2CO_3 buffered $CDCl_3$) δ 181.6, 149.0, 146.4, 143.9, 138.8, 134.6 133.9, 132.2, 129.6, 129.0, 126.9, 126.6, 124.0, 122.1, 120.8, 112.2, 21.4 (Data S20).

(*E*)-1-(1*H*-benzo[*d*]imidazol-2-yl)-3-(3-hydroxyphenyl)prop-2-en-1-one (A)—

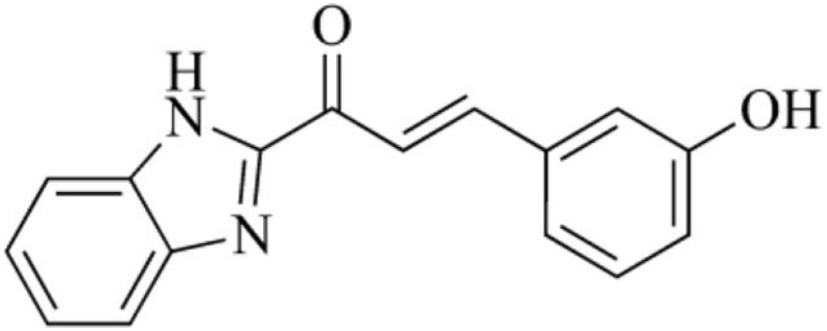

Enone A was synthesized according to General Procedure 1. 4 M aq. NaOH (1.25 mL, 5.00 mmol) was added to 1-(1*H*-benzo[*d*]imidazol-2-yl)ethan-1-one (200 mg, 1.25 mmol) and 3-hydroxybenzaldehyde (166 mg, 1.37 mmol) dissolved in EtOH (2.50 mL). **Enone A** was isolated as a yellow powder after silica gel column chromatography (20–30% EtOAc/hexanes) to afford 78 mg (24% yield). **^{1}H NMR** (500 MHz, DMSO–d_6) δ 13.47 (brs, 1H), 9.69 (brs, 1H), 8.03 (d, *J* = 16.1 Hz, 1H), 7.87 (d, *J* = 16.1 Hz, 1H), 7.87 (brs, 1H), 7.59 (brs, 1H), 7.36 (brs, 2H), 7.31–7.26 (m, 2H), 7.22 (s, 1H), 6.91–6.89 (m, 1H); **^{13}C{1H} NMR*** (125 MHz, DMSO–d_6) δ 180.9, 157.8, 149.0, 144.3, 135.5, 130.2, 121.3, 120.2, 118.5, 114.6 (Data S21).

2-(3-methyl-3*H*-diazirin-3-yl)ethyl 4-methylbenzenesulfonate (B)—

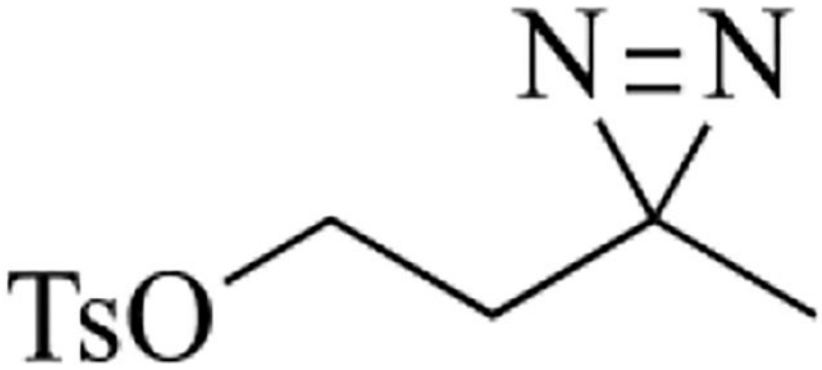

Tosylate B was synthesized in two steps from 4-hydroxybutan-2-one using a known procedure and spectral data were consistent with those previously reported (Kambe et al., 2014).

(*E*)-1-(1*H*-benzo[*d*]imidazol-2-yl)-3-(3-(2-(3-methyl-3*H*-diazirin-3-yl)ethoxy)phenyl)prop-2-en-1-one (UCI-LC0045)—

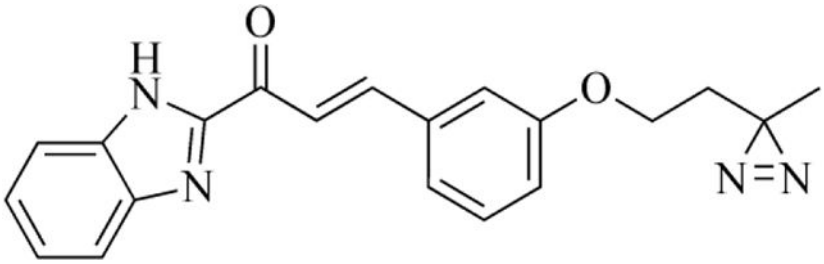

UCI-LC0045 was synthesized by adding 1 M KOH (0.80 mL, 0.80 mmol) to a solution containing **enone A (**61 mg, 0.23 mmol**)** and **tosylate B** (70 mg, 0.28 mmol) dissolved in DMF (1 mL) at rt. The reaction mixture was stirred for 3 days and was then acidified to pH ~7, diluted with EtOAc (20 mL) and washed with sat. aq. brine (3 × 20 mL). The organic layer was dried with Na_2SO_4 and concentrated to afford a yellow-orange amorphous solid. The material was further purified by silica gel column chromatography (15–25% EtOAc/hexanes) to afford **UCI-LC0045** as a pale yellow amorphous solid 20 mg (24% yield). **^{1}H NMR** (500 MHz, K_2CO_3 buffered $CDCl_3$) δ 10.84 (brs, 1H), 8.12 (d, *J* = 16 Hz, 1H), 8.05 (d, *J* = 16 Hz, 1H), 7.96 (d, *J* = 6.6 Hz, 1H), 7.59 (d, *J* = 5.6 Hz, 1H), 7.44 (m, 1H), 7.39 (m, 1H), 7.34 (m, 2H), 7.28 (s, 1H), 7.00–6.99 (m, 1H), 3.93 (t, J = 6.2 Hz, 2H), 1.85 (t, J = 6.2 Hz, 2H), 1.15 (s, 3H); **^{13}C{1H} NMR** (125 MHz, K_2CO_3 buffered $CDCl_3$) δ 181.6, 159.1, 148.9, 146.0, 143.8, 136.0, 134.0, 130.1, 126.7, 124.0, 122.7, 122.1, 121.3, 118.1, 114.1, 112.3, 63.3, 34.5, 24.4, 20.4 (Data S22).

Supplementary Material

Refer to Web version on PubMed Central for supplementary material.

Acknowledgments:

We thank Stacey Borrego for her inputs and guidance in analysis of Nanostring data. We thank the University of California's Experimental Tissue Resource for their assistance with immunohistochemistry of mouse tumor

xenograft tissues. This project was supported by NIH (R01CA11256), NIH (R01GM132826), DOD (BC140911), UL1 TR0001414, and the P30CA062203 Cancer Center Support Grant.

Data and materials availability:

All data is available in the main text or the supplementary materials.

References

Aggarwal M, Saxena R, Sinclair E, Fu Y, Jacobs A, Dyba M, Wang X, Cruz I, Berry D, Kallakury B, et al. (2016). Reactivation of mutant p53 by a dietary-related compound phenethyl isothiocyanate inhibits tumor growth. Cell Death Differ.

Bargonetti J, and Prives C (2019). Gain-of-function mutant p53: History and speculation. J. Mol. Cell Biol.

Baronio R, Danziger SA, Hall LV, Salmon K, Hatfield GW, Lathrop RH, and Kaiser P (2010). All-codon scanning identifies p53 cancer rescue mutations. Nucleic Acids Res 38, 7079–7088. [PubMed: 20581117]

Beraza N, and Trautwein C (2007). Restoration of p53 function: a new therapeutic strategy to induce tumor regression? Hepatology 45, 1578–1579. [PubMed: 17538933]

Blanden AR, Yu X, Loh SN, Levine AJ, and Carpizo DR (2015). Reactivating mutant p53 using small molecules as zinc metallochaperones: Awakening a sleeping giant in cancer. Drug Discov. Today.

Brosh R, and Rotter V (2009). When mutants gain new powers: News from the mutant p53 field. Nat. Rev. Cancer.

Bykov VJ, Issaeva N, Shilov A, Hultcrantz M, Pugacheva E, Chumakov P, Bergman J, Wiman KG, and Selivanova G (2002). Restoration of the tumor suppressor function to mutant p53 by a low-molecular-weight compound. Nat Med 8, 282–288. [PubMed: 11875500]

Bykov VJ, Issaeva N, Zache N, Shilov A, Hultcrantz M, Bergman J, Selivanova G, and Wiman KG (2005). Reactivation of mutant p53 and induction of apoptosis in human tumor cells by maleimide analogs. J Biol Chem 280, 30384–30391. [PubMed: 15998635]

Chen S, Wu J, Liang Y, Lu X, Chen S, and Lu M (2021). Arsenic Trioxide Rescues Structural p53 Mutations through a Cryptic Allosteric Site. Cancer Cell 8, 225–239.

Degtjarik O, Golovenko D, Diskin-Posner Y, Abrahmsén L, Rozenberg H, Shakked Z. (2021). Structural basis of reactivation of oncogenic p53 mutants by a small molecule: methylene quinuclidinone (MQ). Nat Commun 12, 27142–6.

El-Deiry WS, Kern SE, Pietenpol JA, Kinzler KW, and Vogelstein B (1992). Definition of a consensus binding site for p53. Nat. Genet.

Eldar A, Rozenberg H, Diskin-Posner Y, Rohs R, and Shakked Z (2013). Structural studies of p53 inactivation by DNA-contact mutations and its rescue by suppressor mutations via alternative protein-DNA interactions. Nucleic Acids Res. 41, 8748–8759. [PubMed: 23863845]

Freed-Pastor WA, and Prives C (2012b). Mutant p53: one name, many proteins. Genes Dev 26, 1268–1286. [PubMed: 22713868]

Gottlieb A, Althoff K, Grunewald L, Thor T, Odersky A, Schulte M, Deubzer HE, Heukamp L, Eggert A, Schramm A, et al. (2017). RITA displays anti-tumor activity in medulloblastomas independent of TP53 status. Oncotarget.

Habib A-RR, Kajbafzadeh M, Desai S, Yang CL, Skolnik K, and Quon BS (2019). A Systematic Review of the Clinical Efficacy and Safety of CFTR Modulators in Cystic Fibrosis. Sci. Rep. 9, 7234. [PubMed: 31076617]

Jain AN (2007). Surflex-Dock 2.1: Robust performance from ligand energetic modeling, ring flexibility, and knowledge-based search. J. Comput. Aided. Mol. Des.

Kambe T, Correia BE, Niphakis MJ, and Cravatt BF (2014). Mapping the protein interaction landscape for fully functionalized small-molecule probes in human cells. J. Am. Chem. Soc.

Lambert JMR, Gorzov P, Veprintsev DB, Söderqvist M, Segerbäck D, Bergman J, Fersht AR, Hainaut P, Wiman KG, and Bykov VJN (2009). PRIMA-1 Reactivates Mutant p53 by Covalent Binding to the Core Domain. Cancer Cell 15, 376–388. [PubMed: 19411067]

Laptenko O, and Prives C (2006). Transcriptional regulation by p53: One protein, many possibilities. Cell Death Differ.

Leroy B, Fournier JL, Ishioka C, Monti P, Inga A, Fronza G, and Soussi T (2013). The TP53 website: An integrative resource centre for the TP53 mutation database and TP53 mutant analysis. Nucleic Acids Res.

Li T, Kon N, Jiang L, Tan M, Ludwig T, Zhao Y, Baer R, and Gu W (2012). Tumor suppression in the absence of p53-mediated cell-cycle arrest, apoptosis, and senescence. Cell 149, 1269–1283. [PubMed: 22682249]

Liu DS, Duong CP, Haupt S, Montgomery KG, House CM, Azar WJ, Pearson HB, Fisher OM, Read M, Guerra GR, et al. (2017). Inhibiting the system xC- /glutathione axis selectively targets cancers with mutant-p53 accumulation. Nat. Commun. 8.

Lu T, Zou Y, Xu G, Potter JA, Taylor GL, Duan Q, Yang Q, Xiong H, Qiu H, Ye D, et al. (2016). PRIMA-1Met suppresses colorectal cancer independent of p53 by targeting MEK. Oncotarget.

Martins CP, Brown-Swigart L, and Evan GI (2006). Modeling the therapeutic efficacy of p53 restoration in tumors. Cell 127, 1323–1334. [PubMed: 17182091]

Mendez J, and Stillman B (2000). Chromatin Association of Human Origin Recognition Complex, Cdc6, and Minichromosome Maintenance Proteins during the Cell Cycle: Assembly of Prereplication Complexes in Late Mitosis. Mol. Cell. Biol.

Mobaraki RN, Karimi M, Alikarami F, Farhadi E, Amini A, Bashash D, Paridar M, Kokhaei P, Rezvani MR, Kazemi A, et al. (2018). RITA induces apoptosis in p53-null K562 leukemia cells by inhibiting STAT5, Akt, and NF-κB signaling pathways. Anticancer. Drugs.

Molina DM, Jafari R, Ignatushchenko M, Seki T, Larsson EA, Dan C, Sreekumar L, Cao Y, and Nordlund P (2013). Monitoring drug target engagement in cells and tissues using the cellular thermal shift assay. Science (80-.).

Oren M, and Rotter V (2010). Mutant p53 gain-of-function in cancer. Cold Spring Harb. Perspect. Biol.

Patyka M, Sharifi Z, Petrecca K, Mansure J, Jean-Claude B, and Sabri S (2016). Sensitivity to PRIMA-1MET is associated with decreased MGMT in human glioblastoma cells and glioblastoma stem cells irrespective of p53 status. Oncotarget.

Peng X, Zhang MQZ, Conserva F, Hosny G, Selivanova G, Bykov VJN, Arnér ESJ, and Wiman KG (2013). APR-246/PRIMA-1MET inhibits thioredoxin reductase 1 and converts the enzyme to a dedicated NADPH oxidase. Cell Death Dis.

Ran FA, Hsu PD, Wright J, Agarwala V, Scott DA, and Zhang F (2013). Genome engineering using the CRISPR-Cas9 system. Nat. Protoc.

Sanjana NE, Shalem O, and Zhang F (2014). Improved vectors and genome-wide libraries for CRISPR screening. Nat. Methods.

Schneider CA, Rasband WS, and Eliceiri KW (2012). NIH Image to ImageJ: 25 years of image analysis. Nat. Methods 9.

Shimada K, Reznik E, Stokes ME, Krishnamoorthy L, Bos PH, Song Y, Quartararo CE, Pagano NC, Carpizo DR, deCarvalho AC, et al. (2018). Copper-Binding Small Molecule Induces Oxidative Stress and Cell-Cycle Arrest in Glioblastoma-Patient-Derived Cells. Cell Chem. Biol.

Sigal A, and Rotter V (2000). Oncogenic mutations of the p53 tumor suppressor: The demons of the guardian of the genome. Cancer Res.

Sridharan V, Saravanan S, Muthusubramanian S, and Sivasubramanian S (2005). NMR investigation of hydrogen bonding and 1,3-tautomerism in 2-(2-hydroxy-5-substituted-aryl) benzimidazoles. Magn. Reson. Chem.

Sullivan KD, Galbraith MD, Andrysik Z, and Espinosa JM (2018). Mechanisms of transcriptional regulation by p53. Cell Death Differ.

Trott O, and Olson AJ (2009). AutoDock Vina: Improving the speed and accuracy of docking with a new scoring function, efficient optimization, and multithreading. J. Comput. Chem.

Ventura A, Kirsch DG, McLaughlin ME, Tuveson DA, Grimm J, Lintault L, Newman J, Reczek EE, Weissleder R, and Jacks T (2007). Restoration of p53 function leads to tumour regression in vivo. Nature 445, 661–665. [PubMed: 17251932]

Wassman CD, Baronio R, Demir Ö, Wallentine BD, Chen CK, Hall LV, Salehi F, Lin DW, Chung BP, Wesley Hatfield G, et al. (2013). Computational identification of a transiently open L1/S3 pocket for reactivation of mutant p53. Nat. Commun.

Yoshikawa N, Kajiyama H, Nakamura K, Utsumi F, Niimi K, Mitsui H, Sekiya R, Suzuki S, Shibata K, Callen D, et al. (2016). PRIMA-1METinduces apoptosis through accumulation of intracellular reactive oxygen species irrespective of p53 status and chemo-sensitivity in epithelial ovarian cancer cells. Oncol. Rep. 35. 2543. [PubMed: 26986846]

Yu X, Vazquez A, Levine AJ, and Carpizo DR (2012). Allele-Specific p53 Mutant Reactivation. Cancer Cell 21, 614–625. [PubMed: 22624712]

Zache N, Lambert JM, Rokaeus N, Shen J, Hainaut P, Bergman J, Wiman KG, and Bykov VJ (2008). Mutant p53 targeting by the low molecular weight compound STIMA-1. Mol Oncol 2, 70–80. [PubMed: 19383329]

Zhang Q, Bykov VJN, Wiman KG, and Zawacka-Pankau J (2018). APR-246 reactivates mutant p53 by targeting cysteines 124 and 277. Cell Death Dis. 9, 439. [PubMed: 29670092]

Highlights

- Small molecules targeting a cryptic L1/S3 pocket of p53 are identified
- Experimental validation led to the identification of mutant p53 reactivators
- Compounds restore DNA binding of $p53^{MUT}$ in vitro and in vivo
- Compounds directly bind to $p53^{MUT}$ and exert antitumor effect in tumor models

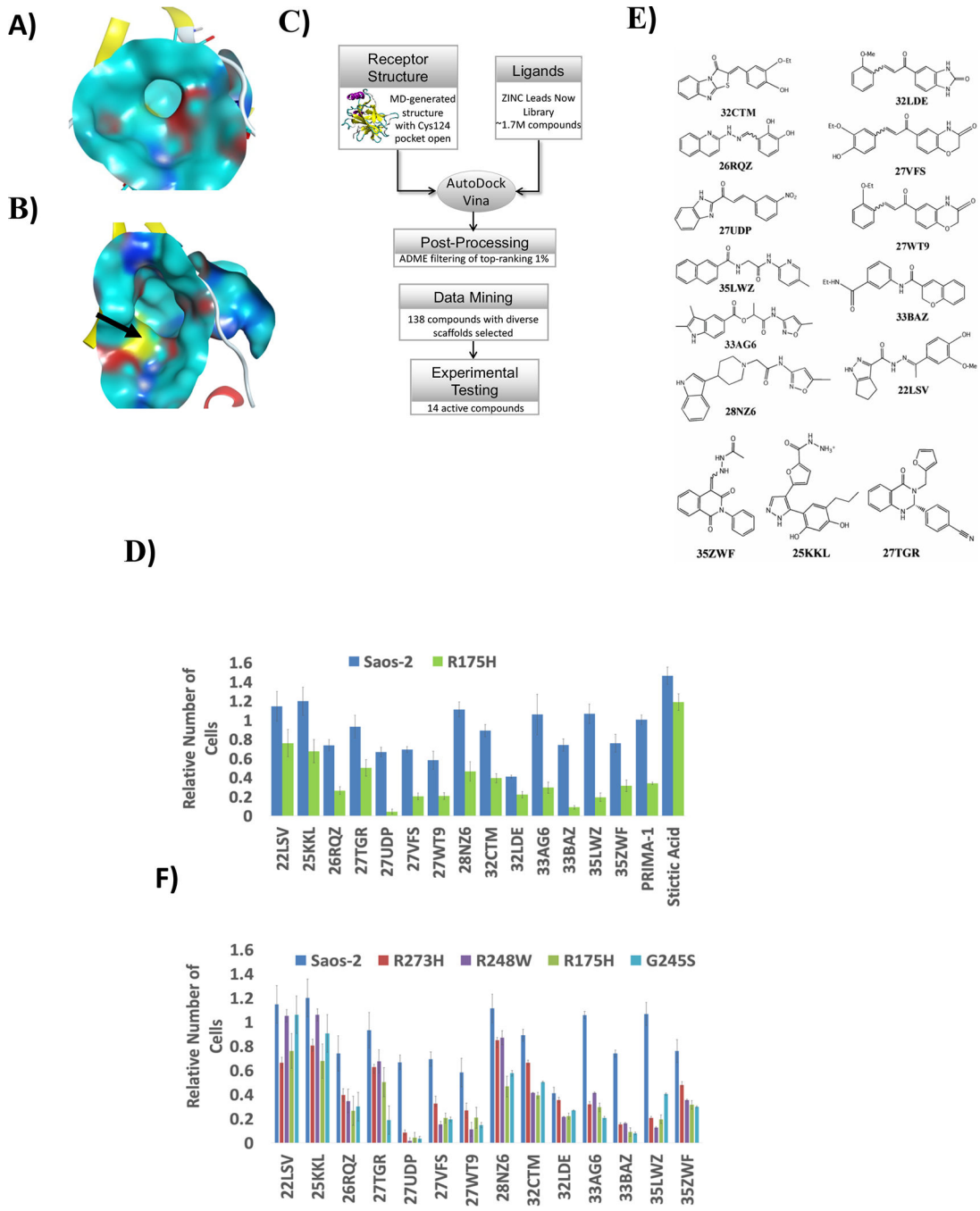

Figure 1: Fourteen potential p53 cancer mutant reactivation compounds.

A) Closed conformation of the L1/S3 pocket in p53 WT crystal structure with pdbID:1TSR, chain B where Cysteine 124 is occluded. **B)** Open conformation of the L1/S3 pocket in a molecular-dynamics-generated frame for the R273H mutant. The black arrow indicates Cysteine 124. The protein surface in panels A and B is colored according to atom types; N: blue, O: red, S: yellow, C: cyan. Secondary structure of the site is depicted in ribbons with beta sheets in yellow, alpha helices in red and loops in white. **C)** A flowchart depicting the virtual screen targeting the L1/S3 pocket of p53**. D)** Saos-2 cells lacking p53 ($p53^{null}$) or

expressing cancer mutant $p53^{R175H}$ were cultured in the presence of different concentrations of computationally predicted reactivation compounds for 3 days. Data is presented as standard error of mean (n= 3). Stictic acid (37μM); 35ZWF, 25KKL, 22LSV, 28NZ6 and 27TGR (100μM); 32CTM (40μM); 26RQZ and 32LDE (10μM); 33AG6 (200μM), 33BAZ (60μM), 27VFS (20μM), 35LVZ, 36EB5 (50μM), and 27UDP (25μM). Data are presented as standard error of mean (n= 3). PRIMA-1 and Stictic acid were previously identified (Lambert et al., 2009; Wassman et al., 2013). **E)** Structures of fourteen computationally predicted p53 reactivation compounds that showed activity in panel D. **F)** Effect of the fourteen predicted compounds on Saos-2 cells ($p53^{null}$) and 4 major p53 cancer mutants ($p53^{R175H}$ $p53^{G245S}$, $p53^{R273H}$, $p53^{R248W}$). Data is presented as standard error of mean (n= 4).

A)

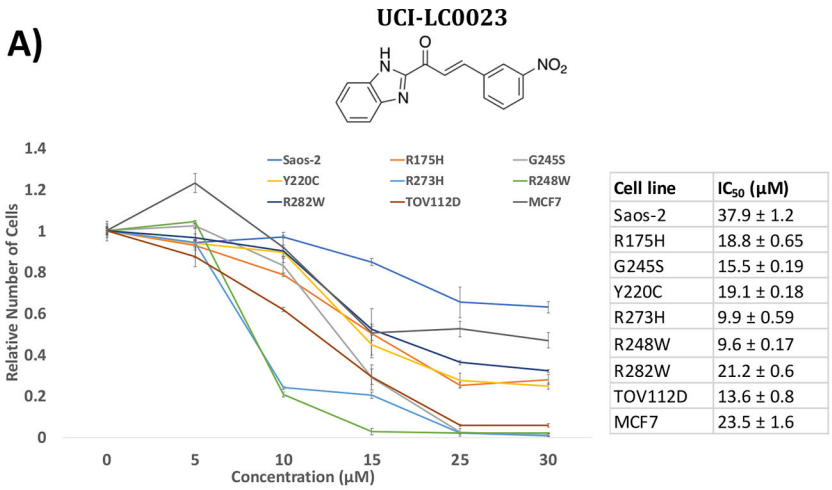

Cell line	IC_{50} (μM)
Saos-2	37.9 ± 1.2
R175H	18.8 ± 0.65
G245S	15.5 ± 0.19
Y220C	19.1 ± 0.18
R273H	9.9 ± 0.59
R248W	9.6 ± 0.17
R282W	21.2 ± 0.6
TOV112D	13.6 ± 0.8
MCF7	23.5 ± 1.6

B)

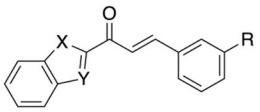

X = S, O, NH
Y = CH, N
R = H, F, Br, CH_3, CF_3, OCH_3

C)

Name	Structure	IC_{50} (μM)		
		Saos-2 ($p53^{null}$)	Saos-2 ($p53^{G245S}$)	TOV112D ($p53^{R175H}$)
UCI-LC0002	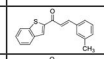	36.7 ± 1.7	26.4 ± 1.1	91 ± 12.1
UCI-LC0003	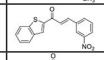	28.7 ± 1.1	32.9 ± 2	34.9 ± 1.9
UCI-LC0005	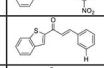	>100	49.9 ± 3.5	>100
UCI-LC0006	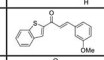	No effect at highest dose	No effect at highest dose	No effect at highest dose
UCI-LC0008	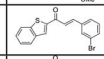	36. 3 ± 0.8	26.3 ± 1	>100
UCI-LC0009	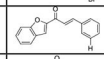	26.8 ± 1.5	20.3 ± 1	26.2 ± 1.6
UCI-LC0010	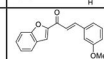	29 ± 0.7	22.9 ± 0.9	20.9 ± 0.5
UCI-LC0012	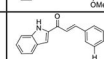	>100	93.9 ± 13.5	59.4 ± 1.2
UCI-LC0013	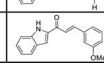	>100	>100	83.9 ± 4.5

Name	Structure	IC_{50} (μM)		
		Saos-2 ($p53^{null}$)	Saos-2 ($p53^{G245S}$)	TOV112D ($p53^{R175H}$)
UCI-LC0014	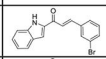	No effect at highest dose	No effect at highest dose	No effect at highest dose
UCI-LC0015	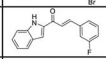	83.6 ± 5.6	35 ± 0.7	84.4 ± 5.7
UCI-LC0016	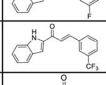	>100	62.4 ± 6.7	55.6 ± 2.1
UCI-LC0018	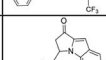	>100	80.1 ± 5.1	>100
UCI-LC0019	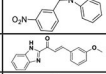	24.1 ± 0.2	16.5 ± 0.8	15.2 ± 0.2
UCI-LC0020		32.5 ± 2	18.8 ± 0.6	20.4 ± 0.3
UCI-LC0021	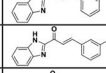	28.8 ± 0.2	18.5 ± 0.5	19 ± 0.6
UCI-LC0022	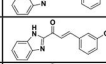	27.6 ± 0.3	18.4 ± 0.4	15.4 ± 0.6
UCI-LC0024	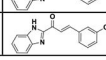	28.8 ± 1.3	18.1 ± 0.3	17.3 ± 0.7

Figure 2: Activity of UCI-LC0023 series of compounds in reactivating p53.

A) Effect of UCI-LC0023 on different p53 cancer mutants. Saos-2 cells lacking p53 ($p53^{null}$) or expressing different p53 mutations ($p53^{R175H}$, $p53^{G245S}$, $p53^{Y220C}$, $p53^{R273H}$, $p53^{R248W}$, $p53^{R282W}$), breast (MCF7) and ovarian cancer (TOV112D) cell lines harboring $p53^{WT}$ and $p53^{R175H}$, respectively, were cultured in the presence of different concentrations of UCI-LC0023 for 3 days. Cell numbers were measured using the CellTiter-Glo® reagent. Data is presented as standard deviation of mean (n= 3). **B)** Structural modifications to

UCI-LC0023. **C)** Structures of UCI-LC0023 derivatives and their corresponding IC_{50} values in Saos-2 cells lacking p53 ($p53^{null}$), expressing $p53^{G245S}$ and TOV112D ($p53^{R175H}$) cells.

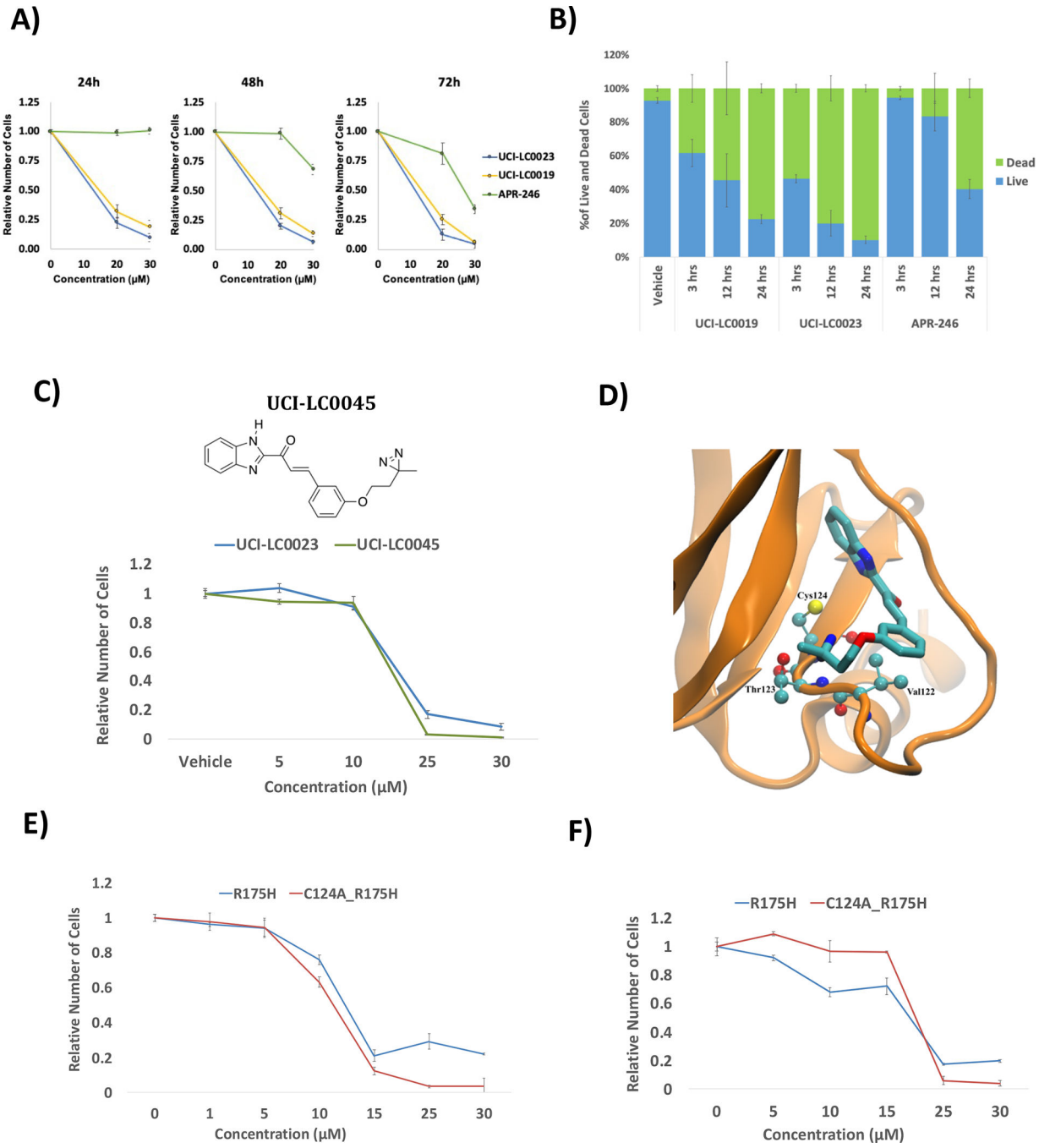

Figure 3: LC0023 directly binds to mutant p53.

UCI-A) TOV112D cells were cultured in the presence of different concentrations of UCI-LC0023, UCI-LC0019 or APR-246 for 24, 48 and 72 hours respectively. Cell numbers were measured using the CellTiter-Glo® reagent. Data is presented as standard deviation of mean (n= 3). **B)** Flow cytometry analysis of TOV112D cells stained with Annexin V and propidium iodide. TOV112D cells were treated with DMSO, 30μM UCI-LC0023, 30μM UCI-LC0019 and 40μM APR-246 for 3, 12 and 24 hours. Data is presented as standard error of the mean (n=3). **C)** Effect of photo-cross linkable diazirine analog UCI-LC0045 and

UCI-LC0023 on TOV112D. Ovarian cancer (TOV112D) cell lines harboring $p53^{R175H}$ were cultured in the presence of different concentrations of UCI-LC0045 and UCI-LC0023 for 3 days. Cell numbers were measured using the CellTiter-Glo® reagent. Data is presented as standard error of mean (n= 3). **D)** Predicted binding pose of UCI-LC0045 in the L1/S3 pocket of $p53^{R175H}$ by docking guided by MS/crosslinking analyses. **E)** Effect of UCI-LC0023 on Saos-2 cells expressing $p53^{R175H}$ and $p53^{C124A\_R175H}$ mutants. Cells were cultured in the presence of different concentrations of UCI-LC0023 for 3 days. Cell numbers were measured using the CellTiter-Glo® reagent. Data is presented as standard deviation of mean (n= 3).

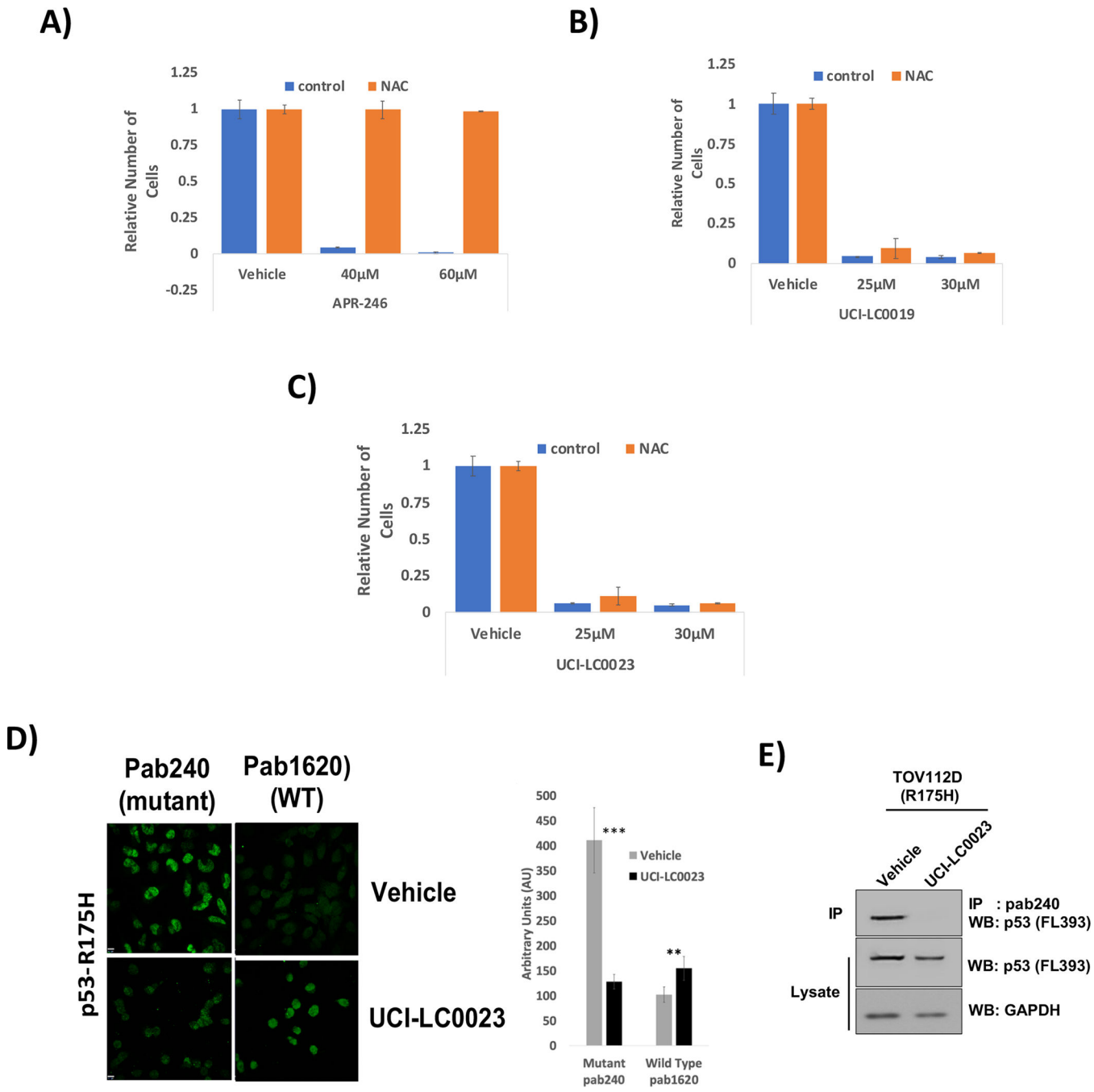

Figure 4: UCI-LC0023 induces conformational changes in p53^{R175H}.

A), B) and C) TOV112D cells were treated with vehicle, 40µM and 60 µM APR-246, 25µM and 30µM UCI-LC0019 and 25µM and 30µM UCI-LC0023 in the presence or absence of 5mM NAC for 3 days. Cell numbers were measured using the CellTiter-Glo® reagent. Data is presented as standard deviation of mean (n=3). **D)** UCI-LC0023 induced conformational changes of p53^{R175H} in ovarian cancer cell line TOV112D, as observed by immunofluorescent staining of cells with p53-conformation selective antibodies PAB240 (mutant conformation) and PAB1620 (WT conformation). All scale bars represent a size

of 10μM. Quantification of PAB240 and PAB1620 staining is shown. Results from two independent experiments with 16 blinded quantified cells are shown in the graph. The error bars represent mean ± S.E.M. ** $p < 0.05$ and *** $p < 0.005$. **E)** Immunoprecipitation of mutant p53 in TOV112D ($p53^{R175H}$) cells using PAB240 antibodies and detection by p53 (FL393) and GAPDH antibodies.

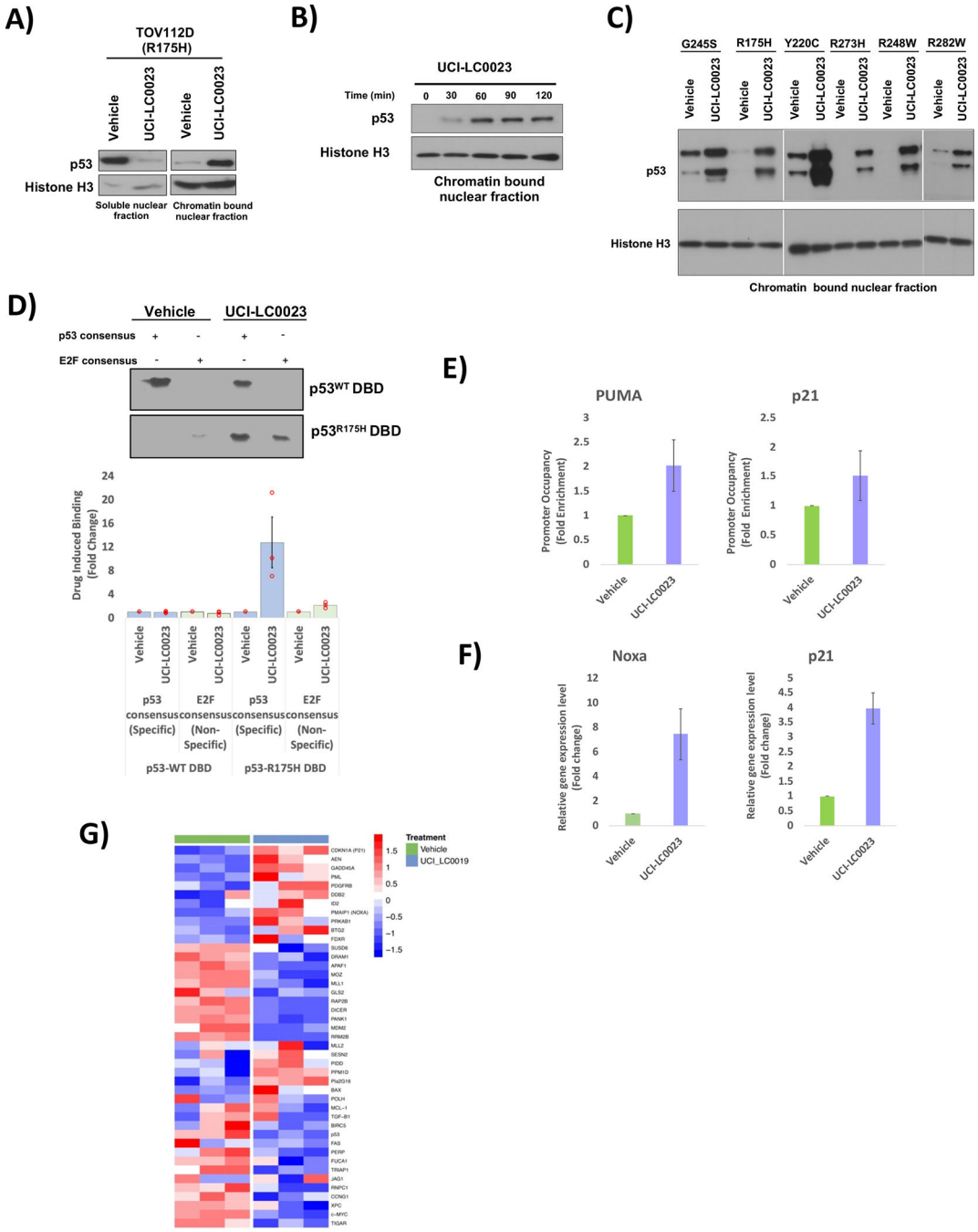

Figure 5: UCI-LC0023 restores DNA binding of p53^{R175H} *in vivo* and *in vitro* and induces p53 target gene expression.

A) and **B)** Cells treated with compound or vehicle were fractionated into cytosolic and nuclear soluble fractions as well as chromatin fractions as indicated by histone H3. UCI-LC0023 restores chromatin binding of p53^{R175H}. **C)** Effect of UCI-LC0023 on chromatin binding of Saos-2 cells expressing different p53 mutations (p53^{R175H} p53^{G245S}, p53^{Y220C}, p53^{R273H}, p53^{R248W}, p53^{R282W}). **D)** Restoration of site-specific DNA binding of mutant p53 in a purified reconstituted system. The recombinant purified DNA binding domains

of $p53^{WT}$ and $p53^{R175H}$ were incubated with biotinylated DNA fragments representing the promoter of the p53-dependent GADD45A gene or a p53 independent (E2F) promoter along with 100 μM UCI-LC0023 or DMSO (vehicle). Protein bound to the DNA fragments was analyzed by immunoblotting with antibodies against p53. Drug induced binding of p53 to p53 consensus and E2F non-consensus sequences is represented as a fold change of UCI-LC0023 treated samples over their respective vehicle controls. **E)** Chromatin immunoprecipitation (ChIP) analysis demonstrates induction of site-specific promoter binding of $p53^{R175H}$ by UCI-LC0023 in TOV112D cells. Eluted DNA was examined by quantitative real time PCR using primers that target the p53 binding site in the promoter regions of p21 and PUMA. Data is represented as standard error of mean (n=3). **F)** q-RTPCR of Noxa and p21 in TOV112D ($p53^{R175H}$) cells treated with 30μM UCI-LC0023 or DMSO (vehicle) for 3 hours. Data is represented as standard deviation of mean (n=3). **G)** p53 target gene expression induced by treatment with 30μM UCI-LC0023 or DMSO (vehicle) in TOV112D ($p53^{R175H}$) cells for 3 hours on a custom p53 nanostring panel. 3 independent experiments are shown as log2 values of the mean.

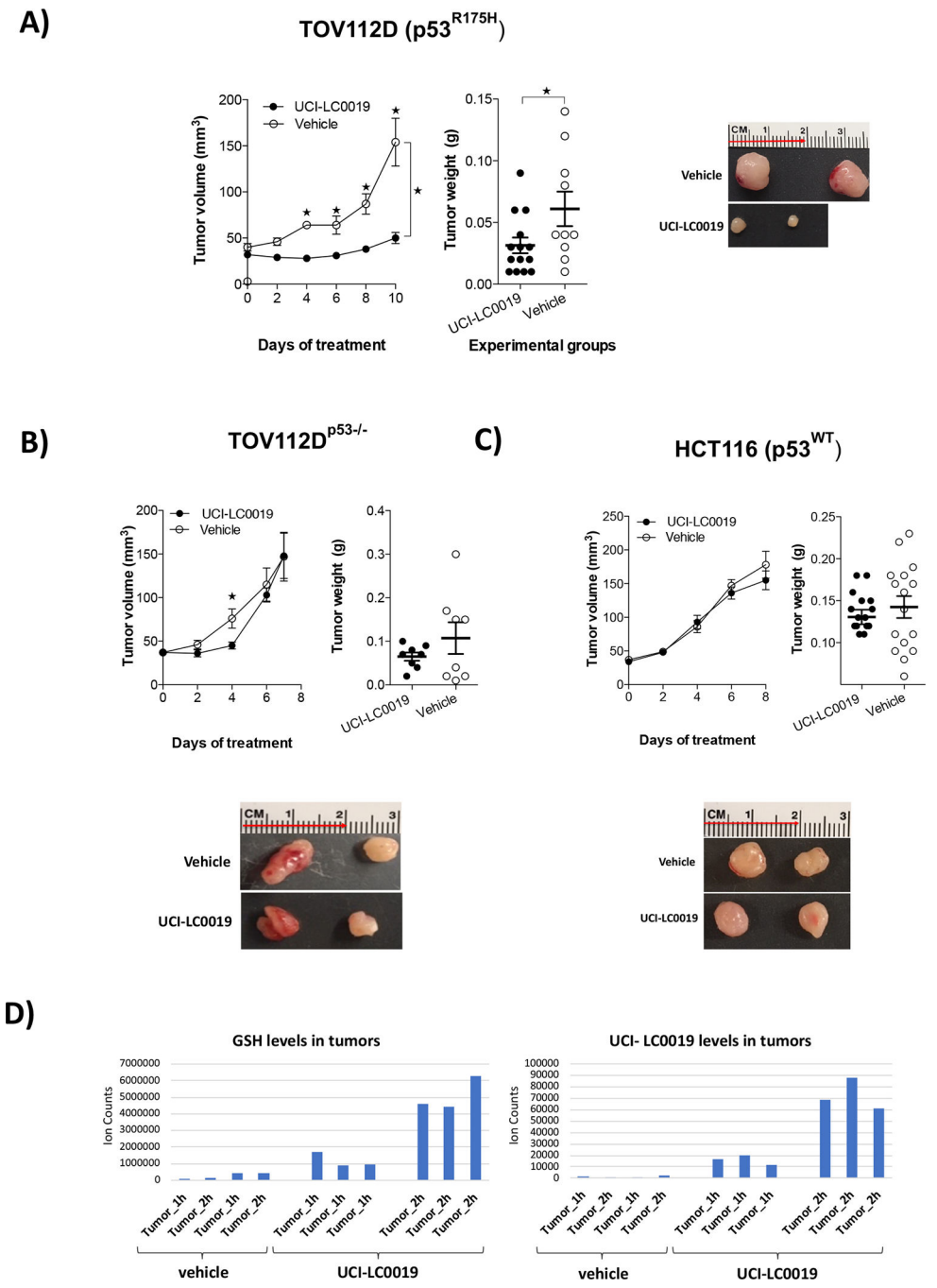

Figure 6: *In-vivo* evidence of UCI-LC0019 mediated p53 reactivation.

A), B), and **C)** Xenograft tumors were generated from TOV112D ($p53^{R175H}$), TOVII2D $^{p53-/-}$ and HCT116 ($p53^{+/+}$). Tumors were allowed to grow to 50mm^3 prior to daily intraperitoneal injections of UCI-LC0019 (10mg/kg). Tumor dimensions were measured every other day and their volumes were calculated by length (L) and width (W) by using the formula: volume = L × W2 × 0.523. The tumor volumes of treated and untreated tumors for TOV112D ($p53^{R175H}$), TOVII2D $^{p53-/-}$ and HCT116 ($p53^{+/+}$) are represented in figures A, B and C. Tumor weight and images of treated and untreated tumors of TOV112D

($p53^{R175H}$), TOVII2D $p53^{-/-}$ and HCT116 ($p53^{+/+}$) are also represented in figures A, B and C respectively. The error bars represent the mean ± SEM * $p<0.05$ by Turkey's multiple comparison test compared to vehicle control. **D)** Mice carrying xenograft tumors (TOV112D [$p53^{R175H}$]) were intraperitoneal injected with vehicle or 10mg/kg UCI-LC0019. Tumors were harvested 1h and 2h after compound injection and intratumor GSH and UCI-LC0019 levels measured by LC-MS.

KEY RESOURCES TABLE

REAGENT or RESOURCE	SOURCE	IDENTIFIER
Antibodies		
p53 (FL-393), rabbit polyclonal Ab	Santa Cruz	Cat #sc-6243
p53 (wild type), clone PAb1620, mouse monoclonal Ab	Merck Millipore	Cat# OP33
p53 (mutant), clone PAb240, mouse monoclonal Ab	Merck Millipore	Cat# OP29
p53 clone DO-1, mouse monoclonal Ab	Active Motif	Cat # 39553
GAPDH (6C5), mouse monoclonal Ab	Santa Cruz	Cat # sc-32233
Anti-Histone H3, rabbit polyclonal Ab	Abcam	Cat # ab1791
Donkey anti-mouse IgG, Alexa Fluor 488	Thermo Fisher	Cat# A-21202
p73 (D3G10), rabbit monoclonal Ab	Cell Signaling Technology	Cat# 14620
p53, Clone D0-7, mouse monoclonal Ab	Agilent Technologies	Cat# M7001
Bacterial and virus strains		
Escherichia coli Rosetta-BL21 (DE3)	Novagen	Cat # 70954-3
Chemicals, peptides, and recombinant proteins		
Dimethyl sulphoxide	Thermo Fisher	Cat# BP231-100
Eprenetapopt (APR-246, PRIMA1-MET)	Selleckchem	Cat# S7724
PRIMA-1	Millipore Sigma	Cat#530050
DMEM without sodium pyruvate	Thermo Fisher	Cat# MT10017CV
Medium 199	Thermo Fisher	Cat# 12-340-030
MCDB 105 medium	Sigma Aldrich	Cat# 117-500
Horse Serum, heat inactivated	Thermo Fisher	Cat# 26050070
2-Acetylbenzothiophene	Combi-Blocks	OR-3695
2-Acetylindole	Combi-Blocks	QC-2113
2-Acetylbenzofuran	Combi-Blocks	OR 1217
2-Acetylbenzimidazole	Combi-Blocks	OR-3940
3-(Trifluoromethyl)benzaldehyde	Combi-Blocks	OR-0670
3-Tolualdehyde	Oakwood Chemicals	001390
3-Methoxybenzaldehyde	Oakwood Chemicals	208834
3-Bromobenzaldehyde	Oakwood Chemicals	003060
3-Fluorobenzaldehyde	Oakwood Chemicals	001668
Benzaldehyde	Alfa Aesar	30749
3-Hydroxybenzaldehyde	Alfa Aesar	A13541
3-Nitrobenzaldehyde	Alfa Aesar	A13594
Leptomycin B	Sigma-Aldrich	L2913
KPT-185	Fisher Scientific	NC0785740
Experimental models: Cell lines		
Human: Saos-2	ATCC	HTB-85
Human: TOV112D	ATCC	

REAGENT or RESOURCE	SOURCE	IDENTIFIER
Human: MCF7	ATCC	HTB-22
Human: HCT116 $p53^{+/+}$	Provided by Dr. Rémi Buisson, University of California, Irvine	N/A
Human: MDA-MB-468	ATCC	HTB-132
Human: MB231	ATCC	HTB-26
Human: HCC70	ATCC	
Experimental models: Organisms/strains		
Female NSG mice	Bred in house	N/A
Recombinant DNA		
lentiviralCRISPRv2	(Sanjana et al., 2014)	Addgene# 52961
pET28a-His-smt3 Thermo	Fisher Scientific	K30001
Software and algorithms		
ImageJ	(Schneider et al., 2012)	https://imagej.nih.gov/ij/
nSolver version 4.0	Nanostring Technologies	https://www.nanostring.com
Volocity	Quorum Technologies	https://quorumtechnologies.com/volocity
ProteinProspector	UCSF Mass Spectrometry Facility	https://prospector.ucsf.edu/prospector/mshome.htm
ChemDraw Professional 12.0	PerkinElmer	https://perkinelmerinformatics.com/products/research/chemdraw/
Autodock Vina	(Trott and Olson, 2009)	http://vina.scripps.edu/index.html
Schrodinger 2012	Schrödinger, LLC	https://www.schrodinger.com
Leadscope	Leadscope, Inc.	www.leadscope.com
Surflex-Dock 2.1	(Jain, 2007)	https://www.biopharmics.com/downloads/
MestReNova	Mestrelab Research	https://mestrelab.com
Other		
Ni-NTA	Qiagen	Cat# 30450
HiTrap Q HP (5 ml)	GE Healthcare	Cat# 17-1154-01
HiTrap SP HP (5 ml)	GE Healthcare	Cat# 17-1152-01
HiLoad 16/600 Superdex 75 pg	GE Healthcare	Cat# 28-9893-33